A Comprehensive Study of Battery-Supercapacitor Hybrid Energy Storage System for Standalone PV Power System in Rural Electrification

Wenlong Jing[a]*, *Chean Hung Lai*[a], *Wallace S.H. Wong*[a], *M. L. Dennis Wong*[b]
[a]Faculty of Engineering, Computing and Science, Swinburne University of Technology Sarawak Campus, Malaysia
[b]School of Engineering and Physical Sciences, Heriot-Watt University, Malaysia
*Corresponding author: wjing@swinburne.edu.my

Abstract - Standalone photovoltaic power system is one of the promising solutions in rural electrification which has been widely implemented to supply electricity for basic household needs. Standalone photovoltaic power systems normally integrate energy storage devices, mainly Lead-acid battery, to compensate the supply-demand mismatch due to the nature of solar energy. However, the short cycle life of Lead-acid battery increases the operating cost of photovoltaic power systems. Supercapacitor-battery hybrid energy storage system has been proposed by researchers to extend the cycle life of battery bank by mitigating the charge-discharge stress due to the fluctuating power exchange. The existing hybrid energy storage systems and their corresponding energy management strategies vary in terms of topology, complexity and control algorithm which are often application oriented. This paper presents a comprehensive review of the state of the art for HESS and discusses potential topologies that are suitable for improving the service life of Lead-acid battery in standalone photovoltaic power systems. Theoretical analysis and numerical simulation in Matlab Simulink for different hybrid energy storage system topologies in rural residential energy system applications have been carried out and their effectiveness in mitigating battery stress are investigated and compared. A battery health cost function is proposed in this paper to quantify the impact of many damaging factors on battery, thus the effectiveness of different hybrid energy storage systems in mitigating battery stress and the associated financial analysis can be quantitatively compared. Finally, a scaled-down hybrid energy storage system prototype has been developed and its performances in standalone photovoltaic system are emulated to validate the simulation analysis.

Index Terms - Battery, Supercapacitor, Hybrid energy storage system, Photovoltaic, Rural electrification, Lifetime extension

I. Introduction

Electricity is one of the essential elements in the development of modern society and economy. The availability of reliable and affordable electricity supply is of crucial importance to people's daily life and economic activities. As of 2015, nearly 1.3 billion people lack access to electricity and over 95% of them live in the developing countries or rural areas [1]. Off-grid rural communities are generally decentralized, lowly populated and isolated from the national grid [2]. Due to resource and financial constraints, it is often difficult to achieve electrification in these areas through the conventional power transmission and distribution approach. A promising solution to address these constraints for rural electrification is distributed autonomous power system based on renewable energy sources and sustainable technologies. Typical renewable energy sources include solar photovoltaic (PV), solar thermal, wind, hydro, biomass, geothermal, ocean waves, and tides, but in recent decades, PV has become one of the most prominent renewable energy technologies attributable to its modularity, easy installation, mature technology and low operating cost [3]. PV applications can be categorized into grid-connected PV system and standalone PV system. Low capacity standalone PV systems are primarily used in off-grid communities to generate electricity for basic electricity needs such as lighting, food refrigeration, and other basic electrical appliances [4, 5].

The typical structure of standalone PV system is presented in Fig. 1, where PV cells are interconnected and encapsulated into modules or arrays that transform solar energy into electricity. The nonlinear electrical characteristic of PV cells and intermittency of solar radiation require integration of intermediate energy storage system (ESS) in order to provide stable electricity supply to the loads. The charge controller, or charge regulator, is used to control the changing process while protecting the battery from overcharge and over discharge. Inverters are used to convert the direct current (DC) power to alternating current (AC) electricity for normal electrical appliances such as lighting, televisions, washing machines, refrigerators etc.

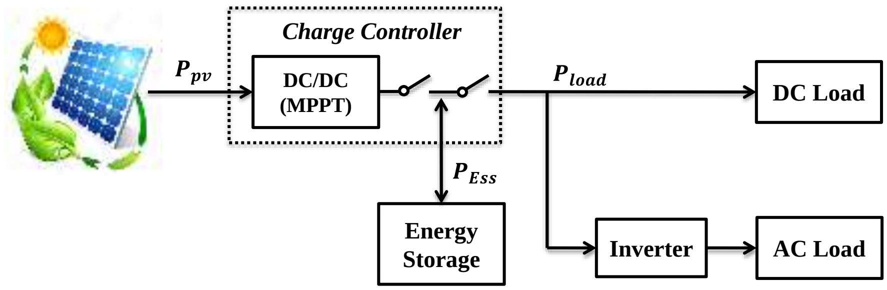

Fig. 1 Typical standalone PV-battery power system

Lithium-ion (Li-ion) and Lead-acid (LA) battery are the two most commonly used ESS technologies in residential energy systems [6]. Li-ion batteries have a higher energy density, better round-trip efficiency, and longer cycle life than LA batteries, but are relatively more expensive and immature in large-scale packaging. In contrast, LA battery bank is more suitable for standalone PV power system especially for rural electrification due to its low cost and better thermal stability. In standalone PV power system, frequent charge-discharge cycles due to generation-demand mismatch causes extra stress on the battery which results in reduced service life [7, 8]. Hybridization of different ESS technologies turns out to be one of the promising ways to mitigate the battery charge-discharge stress by directing the short term power fluctuation to another form of ESS such as the supercapacitor (SC) [9–11]. The SC stores electricity via electrons in static electric field and possesses high power density, has short charging-discharging time, and nearly unlimited cycle life [12].

In battery-SC hybrid energy storage system (HESS), the net current exchange will be decomposed into two or more frequency components. The primary large battery bank will supply the low frequency component which often represents the nominal current profile. As a high power density ESS, the SC absorbs the high frequency power exchange due to the intermittency of solar power and sudden change in load demand. Many variation of HESS and its associated energy management system have been proposed by researchers over the past decades [13–18]. These HESS designs are normally intended to serve large-scale utilities, smart-grid, electric vehicles and other high power applications, and they require extensive sensing, computation, and communication, which significantly increase the system complexity and implementation. However, the study on HESS for off-grid residential energy system especially in rural electrification application is limited because the design considerations for off-grid HESS in the remote areas have not been systematically discussed. This paper aims to address this gap in the literature by presenting a comprehensive review and discussion on the potential HESS topologies and power management strategies in rural electrification applications. It is hoped that this study will ultimately help to accelerate the HESS concept applications in rural standalone PV power systems and relieve economic burden of the local people via primary battery lifetime extension. The targets HESS topologies are iteratively presented and discussed in the sequence from the simplest passive structure to complex active topology. Theoretical analysis and numerical simulation of selected HESS are presented to demonstrate the feasibility and effectiveness of mitigating battery stresses in standalone PV power system based on case studies of a remote community in Sarawak, Malaysia. Novel evaluation method based on a cost function is proposed to compare and to visually display the improvement of HESS on primary battery lifetime. Experiments have been carried out and presented to verify the theoretical analysis.

The rest of paper is organized as follows: section II presents the literature review of battery-SC HESS topologies and energy management strategies; section III presents the mathematical models and analysis of typical standalone PV power system with different HESS topologies; section IV presents the numerical simulation results of different HESSs, followed by battery health cost analysis and comparison; section V demonstrates the HESS prototype developed in this work and presents the experimental results to validate the simulation analysis; and finally, the conclusion is presented in section VI.

II. HESS LITERATURE REVIEW

A. Battery-SC HESS Topologies

Several types of battery-SC HESS topologies have been proposed in various applications aiming to optimally exploit the benefits of different ESS elements [19]. All kinds of various existing or future HESS topologies can be categorised based on the number of ESS elements, the strategies of power-sharing among ESS elements and interfacing methods, as Fig.2 shown.

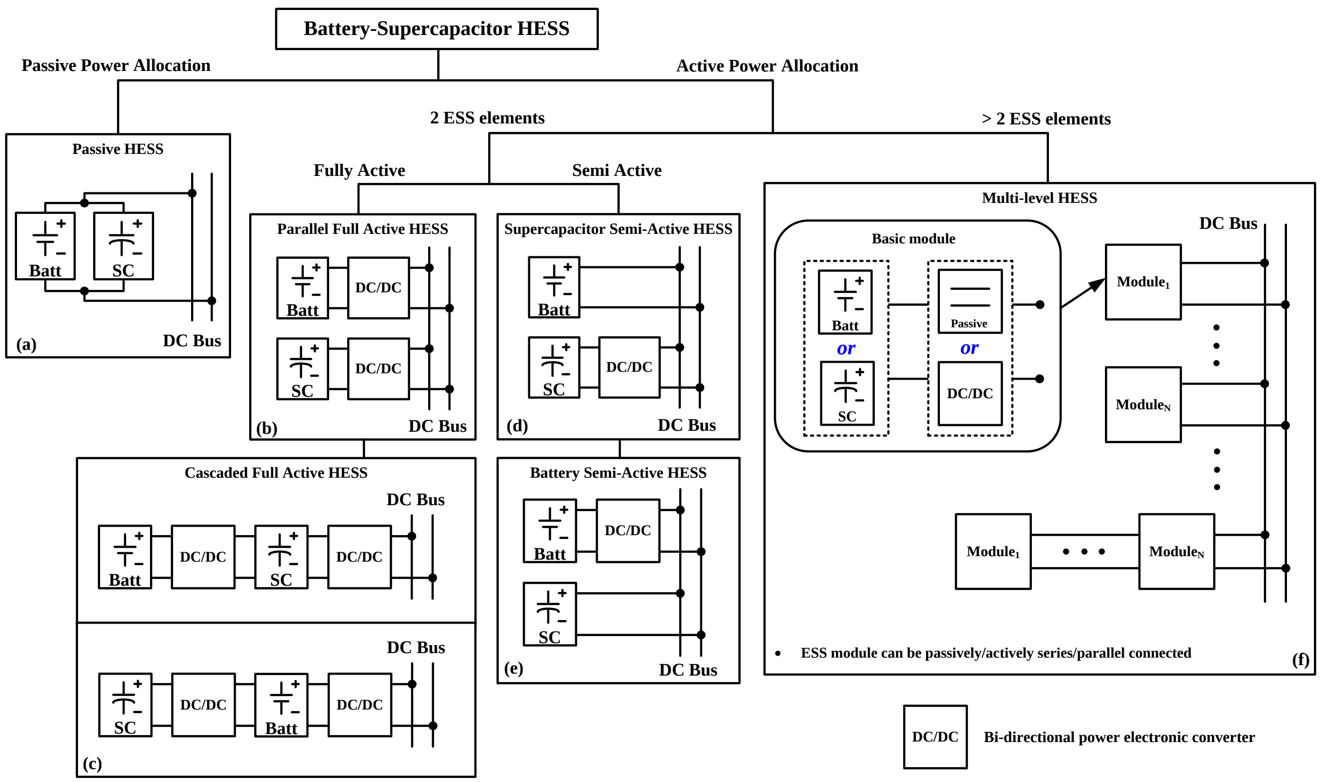

Fig. 2 Classification of Battery-SC HESS topologies

Battery-SC HESS can be configured in passive, active or the combination of both either in parallel or in series. For passive connection, the terminals of ESS are directly connected to the DC bus for which the power sharing mechanism and response is purely determined by the electrical characteristic of the ESS devices. On the other hand, active HESS topologies employ active components such as bi-directional DC/DC power converter to interface the ESS elements from DC bus and to actively control their power flow. Fig. 2(a) shows the simplest form of battery-SC HESS in which the battery and SC are both passively connected to the common DC bus. In this configuration, there is no active component added to the system and the power sharing among battery and SC is determined by the devices' time constants. The drawback of passive HESS is that the capacity of SC cannot be fully utilized due to the different terminal voltage characteristics of battery and SC, resulting in low volumetric efficiency as well as the flexibility in HESS design. It is the earliest concept of HESS topology and rarely used in real applications [20–22].

Isolating ESS element with bi-directional DC/DC converter allows active control of power flow among ESS elements and enables more flexible system configuration settings. The actively controlled ESS modules can be connected in parallel (Fig. 2(b)) or cascaded (Fig.2(c)). The fully active topology can achieve a good control effect, but normally at the expense of system complexity, efficiency, and financial cost. In the parallel full active HESS topology, the power flow of both battery and SC are controlled by individual bi-directional DC/DC converter while regulating the DC bus voltage. The two ESS elements are independent with their own voltage and isolated from DC bus. This feature has caused the parallel full active HESS to be widely discussed and developed by researchers with various energy management algorithms [23–25]. Conversely, cascaded full active HESS has the battery and SC arranged in series as shown in Fig. 2(c). The two DC/DC converters are cascaded controlled with different voltage rate which relatively increases the controller complexity. In general, full active HESS topologies have the advantages that the power flow of each individual ESS element can be performed and controlled optimally based on the designed power allocation strategy. However, the weaknesses of full active HESSs are the high initial cost and system robustness. Since all ESS elements are interfaced by DC/DC converters, the power rating requirement of the electronic components is usually high for energy storage applications such as electric vehicle and residential energy system, leading to significant increase in the overall system cost. Due to the same reason, power systems that employ full active HESS are highly dependent on the actively controlled DC/DC converters and the associated control system to ensure reliable operation.

Semi-active HESS topologies as shown in Fig. 2(d) and Fig. 2(e) have been proposed to exploit the benefits of both passive and active ESS module while compensating the shortcomings of both strategies [26]. For SC semi-active HESS (Fig. 2(d)), the SC module is controlled by using bi-directional DC/DC converter, while the battery module is passively connected to the DC bus. In this setting, the SC terminal voltage is allowed to vary in a wider range which improving the volumetric efficiency. In most cases, the SC will be programmed to absorb short term high frequency fluctuation in DC bus, while the passively connected battery bank will supply the nominal energy requirement of the power system and at the same time maintaining the DC bus voltage passively thanks to the narrow variation in terminal voltage. In addition, the passive battery bank connection enhances the robustness of the power system due to the stable electrical characteristics of battery. Similar to [27], it uses Semi-SC HESS to release the negative impact on the Li-ion battery in EV for the frequent power surges. Conversely, the battery semi-active HESS (Fig. 2(e)) interfaces battery module with bi-directional DC/DC converter and passively couples the SC module with the DC bus [28]. Because of the linear voltage-capacity characteristic, wide and instability in DC bus voltage is expected which could be an issue in many applications. However, the major weakness of this topology is the low volumetric efficiency of SC usage. The installation of SC needs to be large enough to satisfy the wide range of DC bus voltage.

Assuming a basic module includes either or both batteries and SC with/without DC/DC converters, hybridization beyond two ESS modules can be configured in different combinations of passive, active, cascaded and/or parallel with unique power management system and control strategy as depicted in Fig. 2(f) [29–31].The SC or battery can be modularized into different voltage or power levels and performs a good adaptability to different system requirements. *Ye et al.* presented a novel SC cell circuit to overcome the issues of existing imbalance among cell voltages among a large number of series connected battery cells. Its topology is one example of SC-Battery HESS in Fig. 2(f) [32]. This enables a more flexible HESS in terms of system configuration and the adaptability to more sophisticated energy management system for broader power and energy applications.

B. Power Allocation Strategies

Other than the design of HESS topology, the way of power allocation among ESS elements is another critical aspect that determines the effectiveness of HESS in mitigating charge/discharge stress on battery [33]. Fig. 3 depicts a typical energy management system (EMS) structure for HESS in standalone PV applications. The section of high-level control performs power allocation algorithm in microprocessors and collects various information such as the values of real time voltage or current from DC bus and ESS elements, their SoC, weather condition, solar irradiance, load profile etc., while the low-level control manages the current flow in and out of ESS elements based on the signal generated from high-level control.

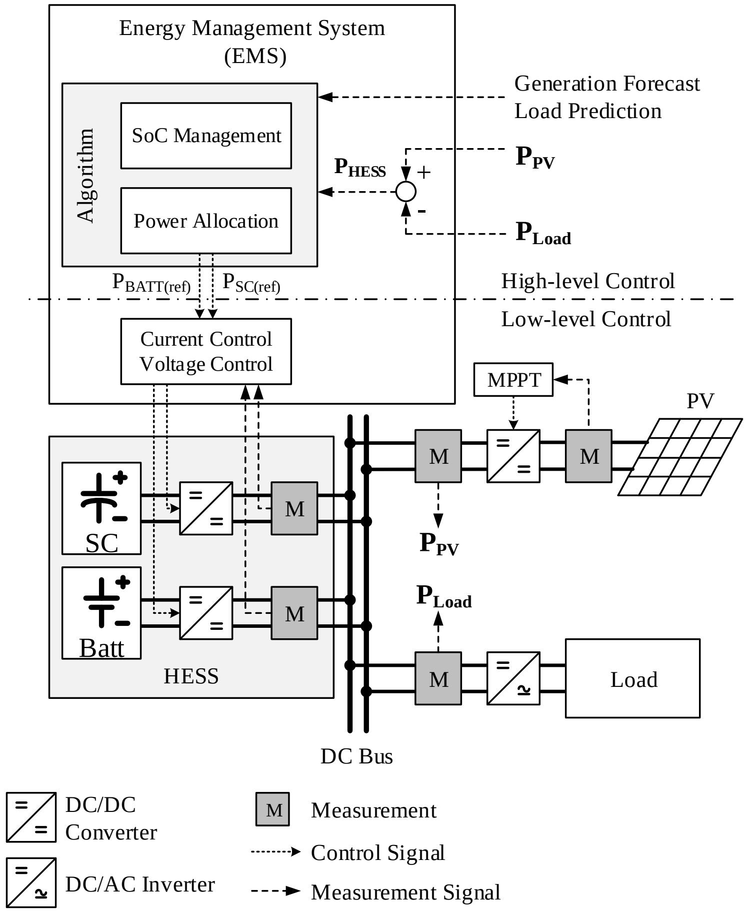

Fig. 3 Typical EMS Structure for Standalone PV power system with Parallel Active HESS [33]

The available power sharing methods can be broadly categorised into non-computational method, rule-based method and intelligent algorithms based method. The typical non-computational method is the usage of low-pass filter. In *Lee et* al's study, it proposed a battery-SC semi-active HESS in standalone PV power system with the control strategy comprising a low-pass filter and fuzzy logic control [34].

The low-pass filter decomposes the net power demand into different frequency components and the fuzzy logic control further minimizes the peak current demand on battery while managing the SC state-of-charge. The membership function of fuzzy logic control is optimized by particle swarm optimization algorithm which demonstrates optimal peak current reduction in battery. The simulation study shows that the proposed method effectively reduces the battery peak power and improved the utilization of SC. Similarly, *Zhou et al.* proposed a full active parallel HESS topology with one SC module and multiple battery modules. A simple linear filtering approach is adopted to filter the short term power fluctuation and direct the smoothed power demands to each battery modules based on their respective state-of-charge (SoC). The single SC module is controlled so that it responds to the short term power exchange within the power system [35]. In the same way, *Branislav et al.* presents a low complexity control system to control full active battery-SC HESS, it used low-pass filter to dynamically decompose the current load into high/low components [23]. Rule-based method contains deterministic rule concept and fuzzy logic methods. The former one is simple and reliable, however, its rules are designed according to the initial state of control targets and unable to be changed once confirmed, which will not accurately control the actual conditions of the elements in long-term. Fuzzy logic method can solve the issues and is widely used in recent years. *Xue et al.* proposed a multimode fuzzy-logic power allocation algorithm to address the supply-demand mismatches while optimally distribute power among ESS modules to ensure all ESSs operate within their safe operating range [36]. Another study conducted by Zineb et al. presented a full-active Battery-SC topology to maintain the voltage of DC bus for PV applications. It used the fuzzy logic to manage the power flows between the battery and SC via dynamic adjusting optimal operation modes and thereby, to maintain a continuous supply of the load with acceptable SoC levels from the energy storage devices. [25].

Besides linear filtering and fuzzy-based approach, many intelligent and complex control algorithms are employed to control battery and SC in HESS. *He Yin et al.* proposed a control strategy based on game theory algorithm for the active HESS, where the battery, SC, and a generator are connected to a DC bus through DC/DC converters [37]. In their work, the multi-agent based decentralized control improved the HESS synergy and could be potentially extended to control complicated hybrid energy system with more devices involved. In [38], the power exchange between PV generation, HESS, and the load is controlled by support vector machine load predictive energy management system. The battery and SC are parallel connected with individual DC/DC converters. The method is able to accurately predict load demand and it effectively solves the issue that the SC fails to response the surge load immediately because of DC/DC converter time delay. *Amin et al.* proposed an energy management strategy using model predictive control in fuel cell-battery-SC hybrid power system and the different ESS devices are individually controlled by active DC/DC converters [39]. The control strategy maintains the current of fuel cell and battery while the SC is programmed to compensate the power discrepancy and at the same time regulates the DC bus voltage. The reference currents for the DC/DC converters were generated by model predictive control and then use hysteresis control to track their variation. *Choi et al.* presented a power management system which provides optimal solution to control the current flow in each ESS elements by solving multi-objectives function with boundary parameters found through multiplicative-increase-additive-decrease (MIAD) principle [40]. These power allocation strategies mainly focus on power sharing between ESS elements without considering the long term variation of battery SoC which may deteriorate the battery performance over time. Additionally, the linear programming, dynamic programming, evolutionary methods such as genetic algorithm, simulated annealing, and particle swarm optimization are also reported in the literatures for HESS optimization [41–45]. These methods normally require heavy computation and complex control system, which most of these sophisticated power management approaches are still under technology development and demonstration levels.

C. HESS for Standalone PV Power System in Rural Electrification

The design of battery-SC HESS topologies and energy management strategies vary in terms of performance, complexity and cost which are often application oriented. In general, better performance and flexibility in power management require higher implementation cost and complexity in control system [46]. This paper discusses the practicality of different HESSs in standalone PV power system specifically for rural electrification applications. Unlike any other high power applications, most standalone PV power systems for rural electrification are geographically isolated. As a result of the high maintenance cost and limited technical support, system robustness turns out to be one of the most important considerations when designing HESS. Therefore, fully active HESS topologies may not be suitable for this rural electrification application. Conversely, HESS that can perform basic power management with minimal active components interfacing secondary ESS module(s) will be the preferred choice.

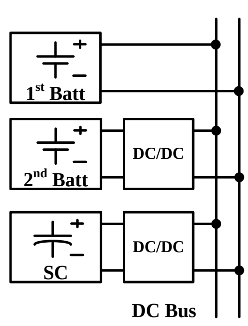

Fig. 4 Three-Level HESS Topology

Among all HESS topologies presented above, the passive HESS (Fig. 2(a)), SC semi-active HESS (Fig. 2(d)), and multi-level HESS configuration with passively connected primary ESS are three potential configurations for standalone PV power system in rural electrification. Based on previous work, a three-level HESS as illustrated in Fig. 4 that extends from the SC semi-active HESS will be discussed and compared with passive and SC semi-active HESSs [47].

III. HESS MODELS

To evaluate and compare the charge-discharge behaviour of the selected HESS designs for rural applications, the responses of different ESS elements are investigated with pulse current loads. Matlab Simulink models of the respective HESS topologies and their control algorithm are developed, and the integration of these HESSs in standalone PV power system are discussed.

A. Passive HESS

For the topology in Fig. 2(a), the response of passive HESS can be modelled by equivalent circuit model as shown in Fig. 5 [48]. The SC is modelled as a large capacitance C with an equivalent series resistance R_{sc} with a finite initial voltage V_{sci} in SC. The LA battery is modeled as a constant voltage source V_{LA} with an equivalent series resistance R_{LA}.

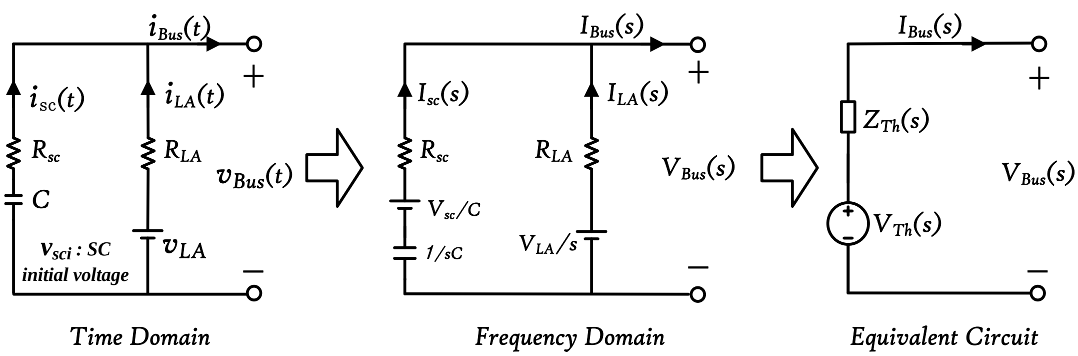

Fig. 5 The equivalent circuit of the passive HESS

The Thevenin equivalent voltage $V_{Th}(s)$ and impedance $Z_{Th}(s)$ in frequency domain are [21][49]:

$$V_{Th}(s)=\frac{R_{LA}}{s}+\frac{R_{LA}}{R_{LA}+R_{sc}}*\frac{v_{sci}-v_{LA}}{s+\frac{1}{(R_{LA}+R_{sc})C}} \tag{1}$$

$$Z_{Th}(s)=\frac{R_{LA}R_{sc}}{R_{LA}+R_{sc}}*\frac{s+\frac{1}{R_{sc}C}}{s+\frac{1}{(R_{LA}+R_{sc})C}} \tag{2}$$

where s is the complex variable. For repetitive pulse load input, the periodic load current, $i_{Bus}(t)$ can be expressed as:

$$i_{Bus}(t)=I_{Bus}\sum_{k=0}^{N-1}[\emptyset(t-kT)-\emptyset(t-(k+D)T)] \qquad (k=0,1,2,\dots) \tag{3}$$

where D is the duty ratio of the input signal, $\emptyset(t)$ is the step function and its Laplace transform in frequency domain is:

$$I_{Bus}(s)=I_{Bus}\sum_{k=0}^{N-1}\left[\frac{e^{-skT}}{s}-\frac{e^{-s(k+D)T}}{s}\right] \qquad (k=0,1,2,\dots) \tag{4}$$

Thus, the voltage-drop across the impedance $Z_{Th}(s)$ for the given current $I_{Bus}(s)$:

$$V_Z(s) = I_{Bus}(s) * Z_{Th}(s) = \frac{R_{LA}R_{sc}I_{Bus}}{R_{LA}+R_{sc}} \sum_{k=0}^{N-1} \left[\frac{s+\frac{1}{R_{sc}C}}{s+\frac{1}{(R_{LA}+R_{sc})C}} * \frac{e^{-skT}-e^{-s(k+D)T}}{s} \right] \quad (5)$$

The terminal voltage in frequency domain can be expressed as:

$$V_{Bus}(s) = V_{Th}(s) - V_Z(s) \quad (6)$$

$$V_{Bus}(s) = \frac{V_{LA}}{s} + \frac{R_{LA}R_{sc}}{R_{LA}+R_{sc}} * \frac{v_{sci}-v_{LA}}{s+\frac{1}{(R_{LA}+R_{sc})C}} - V_Z(s) \quad (7)$$

and its expression in time domain via inverse Laplace transforms:

$$v_{Bus}(t) = v_{LA} + \frac{R_{LA}}{R_{LA}+R_{sc}} * (v_{sci}-v_{LA}) * e^{-\frac{t}{(R_{LA}+R_{sc})C}} - R_{LA}I_{Bus}\sum_{k=0}^{N-1}\left[\begin{array}{c}\left(1-\frac{R_{LA}}{R_{LA}+R_{sc}}e^{-\frac{t-kT}{(R_{LA}+R_{sc})C}}\right)\emptyset(t-kT)\\ -\left(1-\frac{R_{LA}}{R_{LA}+R_{sc}}e^{-\frac{t-(k+D)T}{(R_{LA}+R_{sc})C}}\right)\emptyset(t-(k+D)T)\end{array}\right] \quad (8)$$

Thus the battery current $i_{LA}(t)$ and SC current $i_{sc}(t)$ can be obtained as:

$$i_{LA}(t) = \frac{v_{LA}-v_{Bus}(t)}{R_b} = -\frac{(v_{sci}-v_{LA})}{R_{LA}+R_{sc}} * e^{-\frac{t}{(R_{LA}+R_{sc})C}} + I_{Bus}\sum_{k=0}^{N-1}\left[\begin{array}{c}\left(1-\frac{R_{LA}}{R_{LA}+R_{sc}}e^{-\frac{t-kT}{(R_{LA}+R_{sc})C}}\right)\emptyset(t-kT)-\\ \left(1-\frac{R_{LA}}{R_{LA}+R_{sc}}e^{-\frac{t-(k+D)T}{(R_{LA}+R_{sc})C}}\right)\emptyset(t-(k+D)T)\end{array}\right] \quad (9)$$

$$i_{sc}(t) = i_{Bus}(t) - i_{LA}(t) \quad (10)$$

Since the SC and battery will share the same terminal voltage with DC bus at steady states, where $v_{sci} = v_{LA}$, then their current in steady state are:

$$i_{LAss}(t) = I_{Bus}\sum_{k=0}^{N-1}\left[\begin{array}{c}\left(1-\frac{R_{LA}}{R_{LA}+R_{sc}}e^{-\frac{t-kT}{(R_{LA}+R_{sc})C}}\right)\emptyset(t-kT)-\\ (1-\frac{R_{LA}}{R_{LA}+R_{sc}}e^{-\frac{t-(k+D)T}{(R_{LA}+R_{sc})C}})\emptyset(t-(k+D)T)\end{array}\right] \quad (11)$$

$$i_{SCss}(t) = \frac{R_{LA}I_{Bus}}{R_{LA}+R_{sc}}\sum_{k=0}^{N-1}\left[\begin{array}{c}e^{-\frac{t-kT}{(R_{LA}+R_{sc})C}} * \emptyset(t-kT)-\\ -e^{-\frac{t-(k+D)T}{(R_{LA}+R_{sc})C}} * \emptyset(t-(k+D)T)\end{array}\right] \quad (12)$$

At time $t = (D+k)T$, the pulse load current steps from low to high resulting in a net change in HESS current. Assume the maximum current occurs at *N* approaching infinity, the battery peak current can be simplified as:

$$i_{LAp} = I_{Bus}(1-\varepsilon) \quad (13)$$

where

$$\varepsilon = \frac{R_{LA}}{R_{LA}+R_{sc}} * e^{-\frac{DT}{(R_{LA}+R_{sc})C}} * \frac{1-e^{-\frac{(1-D)T}{(R_{LA}+R_{sc})C}}}{1-e^{-\frac{T}{(R_{LA}+R_{sc})C}}} \quad (14)$$

The parameter ε defines the current sharing relationship between the battery and SC. It indicates that the battery peak current will always be less than I_{Bus} when SC is connected. Equation (13) also expresses the relation between the battery current and DC bus current at specific time. In the case where the LA battery operates under a rated current, the DC bus current can be calculated as:

$$I_{Bus} = \frac{1}{(1-\varepsilon)} I_{LARated} = \partial * I_{LARated} \tag{15}$$

To evaluate the peak power enhancement in HESS, assuming the instantaneous HESS peak power is occurred at rated current:

$$P_{HESSp} = I_{Bus} * V_{Bus} = \partial * I_{LARated} * V_{Bus} = \partial * P_{LARated} \tag{16}$$

It is shown in Equation (16) that the peak power in HESS is increased as the parameter ∂ is larger than 1, with SC connected passively in parallel. The passive HESS model in Matlab Simulink is shown in Fig. 6(a). A 12 Ampere-hour LA battery and 10 Farad SC are connected in parallel to the load. The input pulsed current load is set to 5 Ampere, 50% duty cycle and cycling period of 10 seconds. Fig. 6(b) presents the simulation results of power-sharing between LA battery and SC. At the rising edge, the SC responses rapidly due to the relatively low time constant. On the other hand, the battery slowly picks up over time and supply the demanded current. The results show minor effect on the power-sharing in the passively connected battery-SC HESS for which the power-sharing is only occurred within fractions of second. Additionally, the power-sharing capability of passive HESS is fixed based on the internal parameters of the two ESS elements.

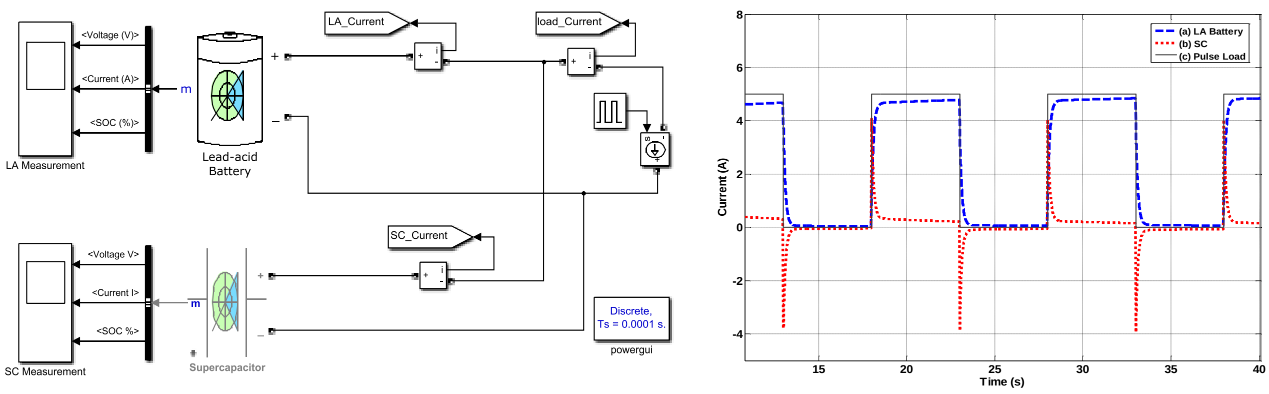

(a) **(b)**

Fig. 6 (a) Matlab Simulink Model of passive HESS, (b) Pulse load response of passive HESS

The integration of passive battery-SC HESS on typical standalone PV power system is illustrated in Fig. 7. The LA battery is normally the primary ESS of choice. The charge controller is modeled as a uni-directional DC/DC converter with maximum power point tracking (MPPT) algorithm and two control switches for interfacing the HESS and load. A diesel/petrol generator is normally integrated as a backup and dispatchable power source in case of system failure or when additional energy is required.

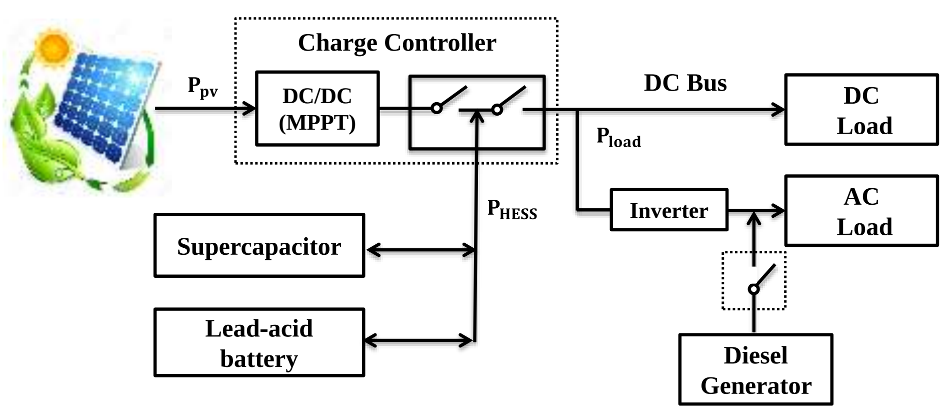

Fig. 7 Standalone PV power system with passive HESS

B. SC Semi-active HESS

The SC semi-active HESS is shown in Fig. 2(d); its equivalent circuit model in the time domain and frequency domain are presented in Fig. 8.

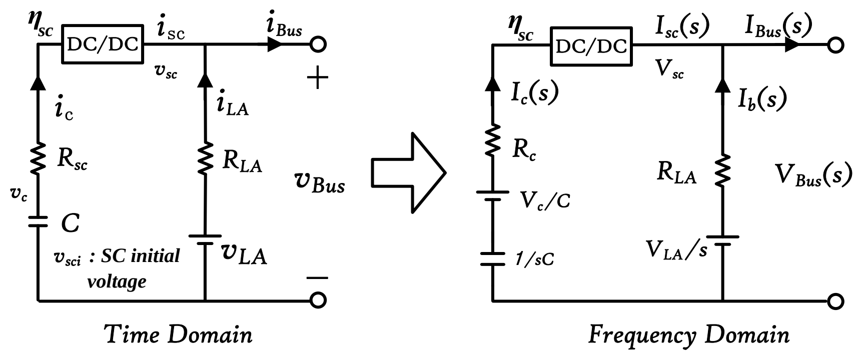

Fig. 8 The equivalent circuit of the SC semi-active HESS

By neglecting the dynamic characteristics, the DC/DC converter is simplified and represented as parameters of efficiency η_{sc} and voltage transfer rate K_{sc} [49]. Thus the SC real time terminal voltage and current before DC/DC converter is expressed as:

$$i_c(t) = \frac{K_{sc}}{\eta_{sc}} i_{sc}(t) = i_{Bus}(t) - i_{Bus}(t)_{LPF} \quad (17)$$

$$v_c = \frac{v_{sc}}{K_{sc}} = \frac{v_{bus}}{K_{sc}} \quad (18)$$

where the $i_{Bus}(t)_{LPF}$ is the filtered $i_{Bus}(t)$. When pulse load $i_{Bus}(t)$ is applied, the SC current and the battery current on DC bus can be expressed as:

$$i_{Bus}(t) = I_{Bus} \sum_{k=0}^{N-1} [\emptyset(t-kT) - \emptyset(t-(k+D)T)] = i_{sc}(t) + i_{LA}(t) \quad (19)$$

$$i_{sc}(t) = \frac{\eta_{sc}}{K_{sc}} i_c(t) = \frac{\eta_{sc}}{K_{sc}} [i_{Bus}(t) - i_{Bus}(t)_{LPF}] \quad (20)$$

$$i_{LA}(t) = I_{Bus} \sum_{k=0}^{N-1} [\emptyset(t-kT) - \emptyset(t-(k+D)T)] - \frac{\eta_{sc}}{K_{sc}} [i_{Bus}(t) - i_{Bus}(t)_{LPF}] \quad (21)$$

Assuming the peak current will occur at the end of the pulse duty cycle, $t = (k+D)T$, and then the maximum current drawn from the battery can be expressed as,

$$i_{LAp} = I_{Bus} - \frac{\eta_{sc}}{K_{sc}} [i_{Bus}(t) - i_{Bus}(t)_{LPF}] \quad (22)$$

It shows that the peak current of battery is reduced by the SC current which is actively controlled by DC/DC converter. As a result, mitigation in battery stress due to surge current can be achieved.

The Matlab Simulink model for SC semi-active HESS has been developed as shown in Fig. 9(a); the parameters for SC, LA battery and the input pulsed current are set identical as presented above. Fig. 9(b) shows the simulation results for power-sharing between LA battery and SC in Semi-active setting. Firstly, the net change in current demand is filtered by the low-pass filter (τ= 1.5s), and the high frequency component will be used to control the current flow in SC. A simple proportional-integral controller is implemented to track the reference signal, while the remaining of the current demand will be responded by the passively controlled LA battery bank. The advantage of actively controlled SC module is that the time constant of the response can be adjusted to better utilize the SC module. Also, the isolation of the SC module from the DC bus allows wider variation in state-of-charge that significantly improves the volumetric efficiency. However, due to the unavoidable time delay of the active component and controller, there is an inrush current when there is a step change in load current.

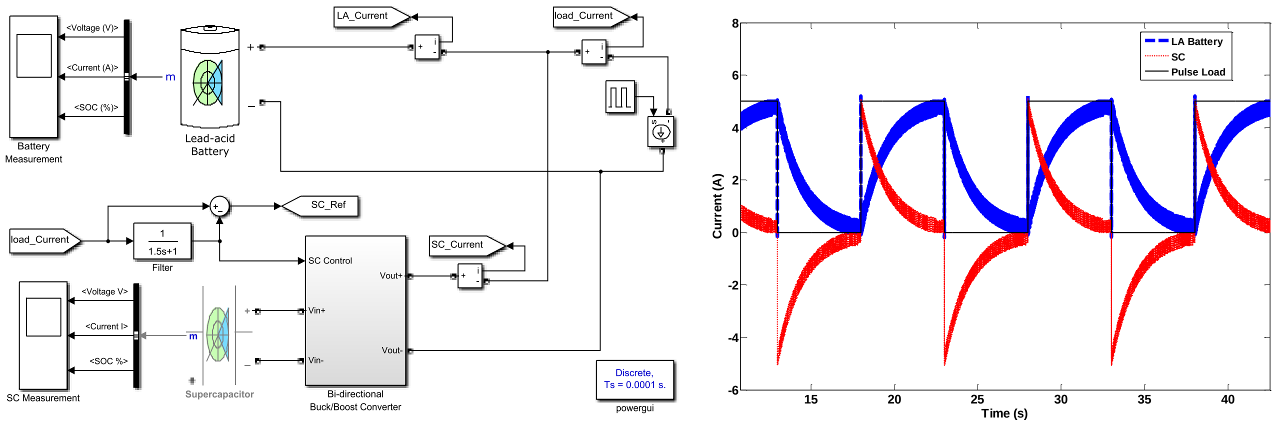

(a) (b)

Fig. 9 (a) The Matlab Simulink model of the SC semi-active HESS, (b) Pulse load response of the SC semi-active HESS

Fig. 10 depicts the same standalone PV power system with SC semi-active HESS as the energy storage. The LA battery is directly connected to the DC bus, while the SC is interfaced with a bi-directional DC/DC converter. The net change in current is measured and a pulse width modulation signal with appropriate duty cycle D_{SC} is generated by the controller to control the power flow of SC.

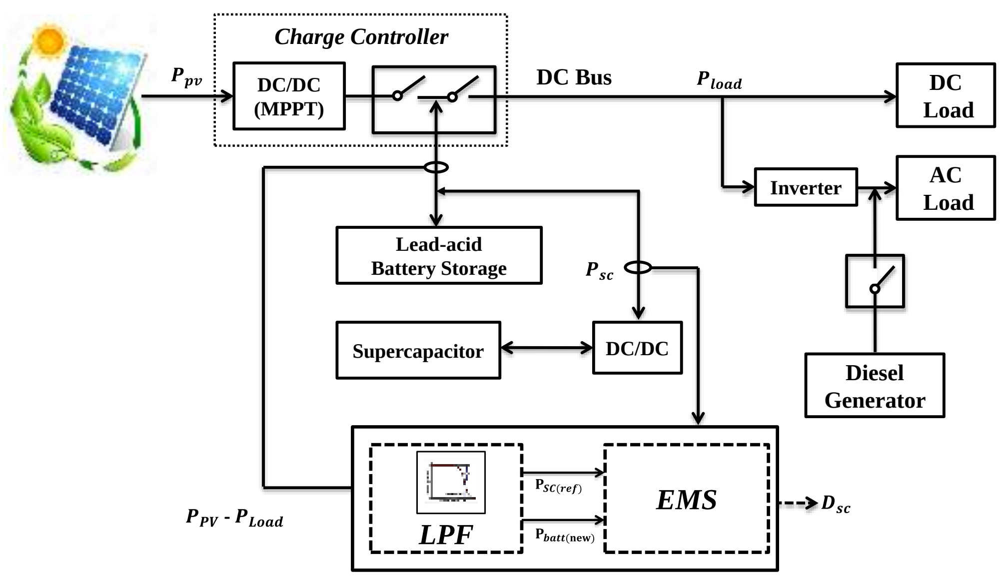

Fig. 10 Standalone PV power system with SC semi-active HESS

A simple control scheme is illustrated in Fig. 11 where the demanded power PHESS is filtered by using low-pass filter and the high-frequency component of the power exchange will be used as the reference signal $P_{SC(ref)}$ for SC. A carefully tuned current tracker (proportional-integral controller) is used to control the power flow from SC. When selecting the bandwidth of the low-pass filter, a trade-off exists between the smoothness of battery current I_{Batt} and the capacity of SC. For instance, a relatively low cut-off frequency in low-pass filter will generate a smoother I_{Batt} but requires larger SC capacity as well as higher power rating of active components in DC/DC converter.

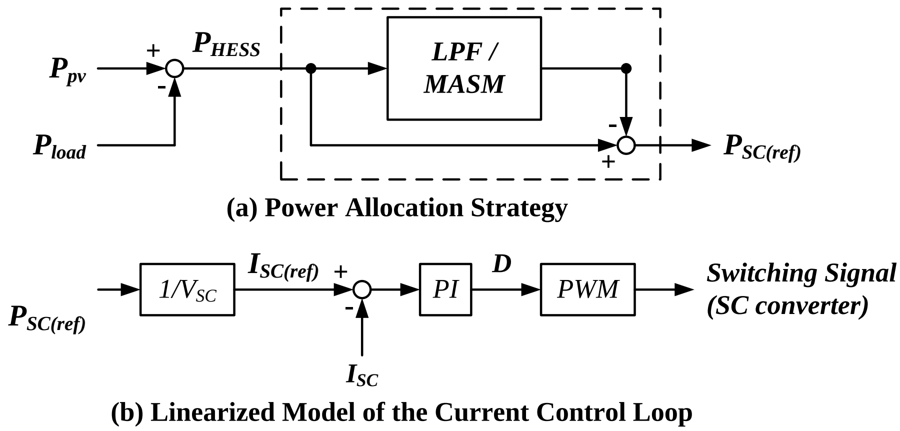

Fig. 11 Power allocation strategy for the SC semi-active HESS

C. Three-level HESS

In order to maximize the advantages of the previous two topologies, this paper proposes the three-level HESS topology. Fig. 12 illustrates the equivalent circuits of the three-level HESS topology.

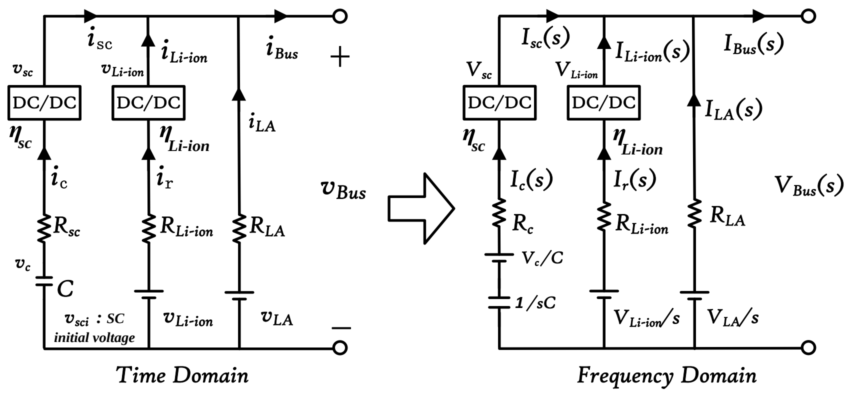

Fig. 12 The equivalent circuit model of the Three-level HESS

The SC terminal voltage and current can be expressed as:

$$v_{sc} = \frac{v_{sc}}{\mathrm{K}_{sc}} = \frac{v_{bus}}{\mathrm{K}_{sc}} \tag{23}$$

$$i_c(t) = \frac{\mathrm{K}_{sc}}{\eta_{sc}} i_{sc}(t) = i_{Bus}(t) - W_1 * i_{Bus}(t)_{LPF1} - \{[i_{Bus}(t) - w_1 * i_{Bus}(t)_{LPF1}]\}_{LPF2} \tag{24}$$

and for the Li-ion battery,

$$v_{Li-ion} = \frac{v_r}{\mathrm{K}_{Li-ion}} = \frac{v_{bus}}{\mathrm{K}_{Li-ion}} \tag{25}$$

$$i_r(t) = \frac{\mathrm{K}_{Li-ion}}{\eta_{Li-ion}} i_{Li-ion}(t) = \{[i_{Bus}(t) - w_1 * i_{Bus}(t)_{LPF1}]\}_{LPF2} \tag{26}$$

where the η_{sc}, η_{Li-ion}, K_{sc} and K_{Li-ion} are the efficiencies and voltage transfer rates of the corresponding DC/DC converters respectively, W_1 is the scaling factor that set the proportion of Li-ion battery capacity in total power demand. For pulse load response, the pulsed input current, LA battery, Li-ion battery and SC currents on are:

$$i_{Bus}(t) = I_{Bus} \sum_{k=0}^{N-1} [\emptyset(t - kT) - \emptyset(t - (k + D)T)] = i_{LA}(t) + i_{Li-ion}(t) + i_{sc}(t) \qquad (27)$$

$$i_{sc}(t) = \frac{\eta_{sc}}{\mathrm{K}_{sc}} i_c(t) \qquad (28)$$

$$i_{Li-ion}(t) = \frac{\eta_{Li-ion}}{\mathrm{K}_{Li-ion}} i_r(t) \qquad (29)$$

$$i_{LA}(t) = I_o \sum_{k=0}^{N-1} [\emptyset(t - kT) - \emptyset(t - (k + D)T)] - \frac{\eta_{sc}}{\mathrm{K}_{sc}} i_c(t) - \frac{\eta_{Li-ion}}{\mathrm{K}_{Li-ion}} i_r(t) \qquad (30)$$

Similarly, assuming the peak power demand still occurs at $t = (k + D)T$, and the maximum current drawn from the LA battery can be expressed in eq. (31) when N tends to infinity,

$$i_{LAp} = I_{Bus} - \frac{\eta_{sc}}{\mathrm{K}_{sc}} i_c(t) - \frac{\eta_{Li-ion}}{\mathrm{K}_{Li-ion}} i_r(t) \qquad (31)$$

Fig. 13(a) depicts the Matlab Simulink model of three-level active HESS. The parameters for LA battery module, SC module and pulse load are kept identical as in the previous cases. The additional Li-ion battery module has a capacity of 2 Ampere-hour and the scaling factor W_1 is set to 0.85. The responses of the Li-ion battery, LA battery, and SC are depicted in Fig. 13(b). The SC is programmed to response to the transient current, while the Li-ion battery responses to the medium frequency component during current variation and supplying a small portion of the current demand. This enables the reduction in peak current for the passive LA battery bank which contributes to the cycle life of the battery.

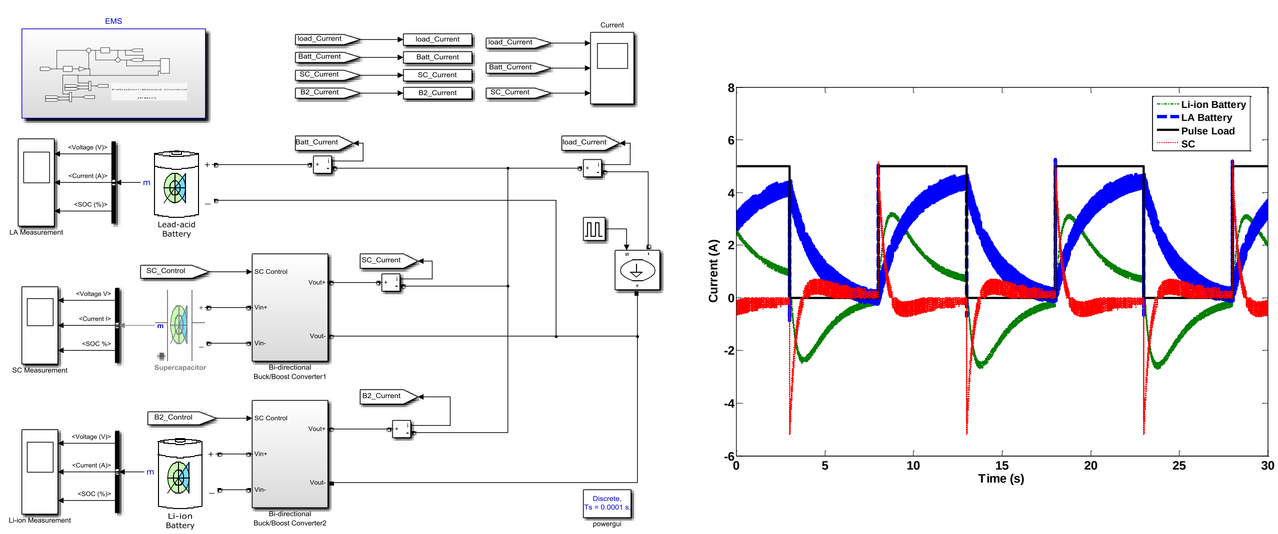

(a) (b)

Fig. 13 (a) The Matlab Simulink model of the three-level active HESS, (b) Pulse load response of the three-level active HESS

Fig. 14 illustrates the standalone PV power system with three-level battery-SC HESS in which three different energy storage devices are utilized for better stress mitigation. In this setting, two actively controlled complementary ESS elements (SC and

Li-ion battery) are connected in parallel with the passively connected primary LA battery. The combination of SC and Li-ion modules enhances the stress mitigation capability by covering a wider spectrum of current fluctuation as well as supply part of the nominal current demand, which enables a more stable charge-discharge process and peak current reduction in the primary LA battery bank. The associated power allocation strategy is shown in Fig. 15. Two low-pass filters are cascaded to decompose the net power demand into three different frequency ranges. The highest frequency $P_{SC(ref)}$ will be used as the reference signal to control the power flow of the SC module. While the medium frequency component $P_{Li\text{-}ion(ref)}$ will be the reference for Li-ion battery module. A scaling factor W_1 is proposed to set the proportion of Li-ion battery load in total power demand.

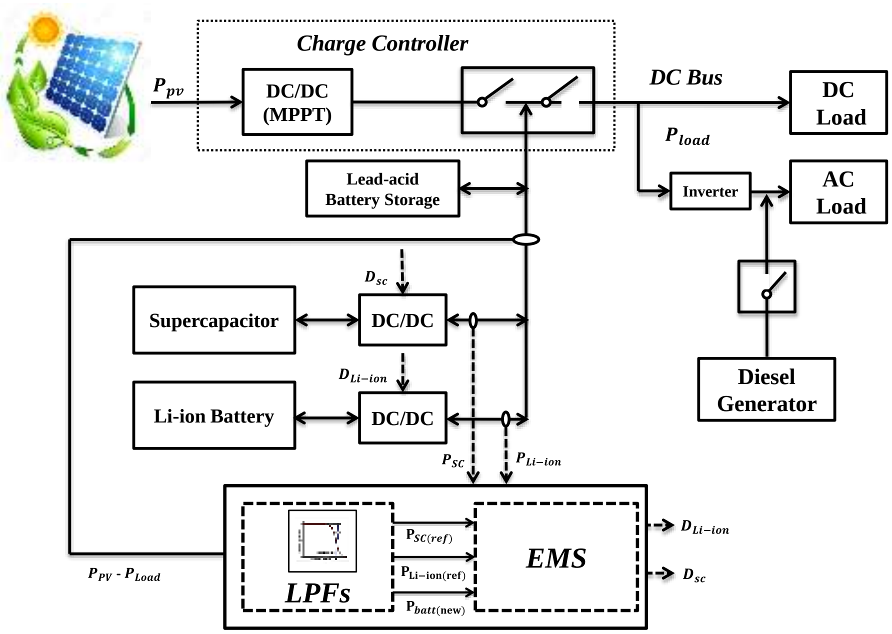

Fig. 14 Standalone PV power system with three level HESS

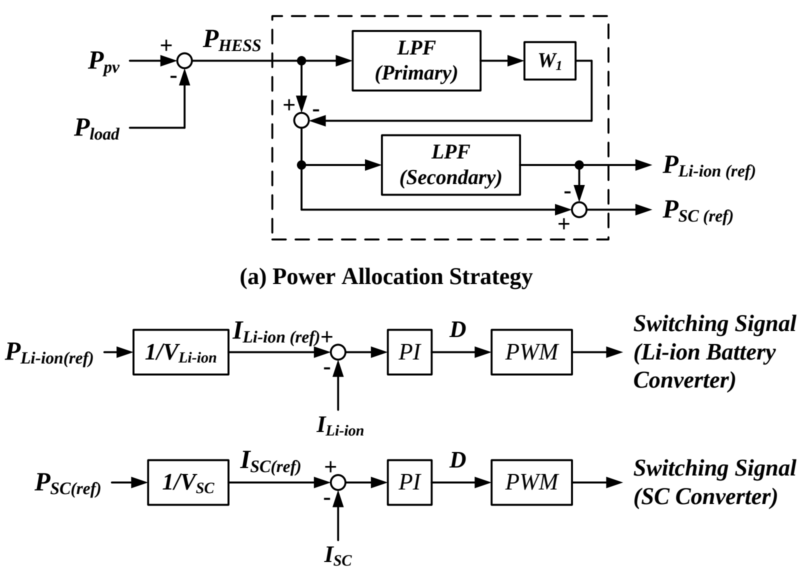

(b) Linearized Model of the Current Control Loop

Fig. 15 Power allocation strategy for the Three-level HESS

IV. CASE STUDY

To evaluate the effectiveness of the selected HESS in mitigating battery stress in standalone PV power system, a Matlab Simulink model of 5kW standalone PV power system is developed and simulations have been carried out with actual solar irradiance data and estimated load profile from a rural community in Sarawak, Malaysia. Fig.16 shows a 24-hour solar irradiance data recorded for a typical (a) sunny day and (b) cloudy day in Kuching, Sarawak. As demonstrated from the graphs, tropical climate in the region generates significant power fluctuations even on a sunny day. These solar irradiance data will be used to generate PV power for the simulation. As to the electricity consumption data, a site survey has been conducted at the selected rural site (1˚14’20.5”N, 112˚02’10.7”E) to collect the information of household and electrical appliances. Based on the behaviour of each electricity user, an estimated load profile is generated as shown in Fig. 16(c). The selected rural site consists of 6 households and 13 electricity users with basic electricity appliances such as lightings, television, radio, refrigerator etc.

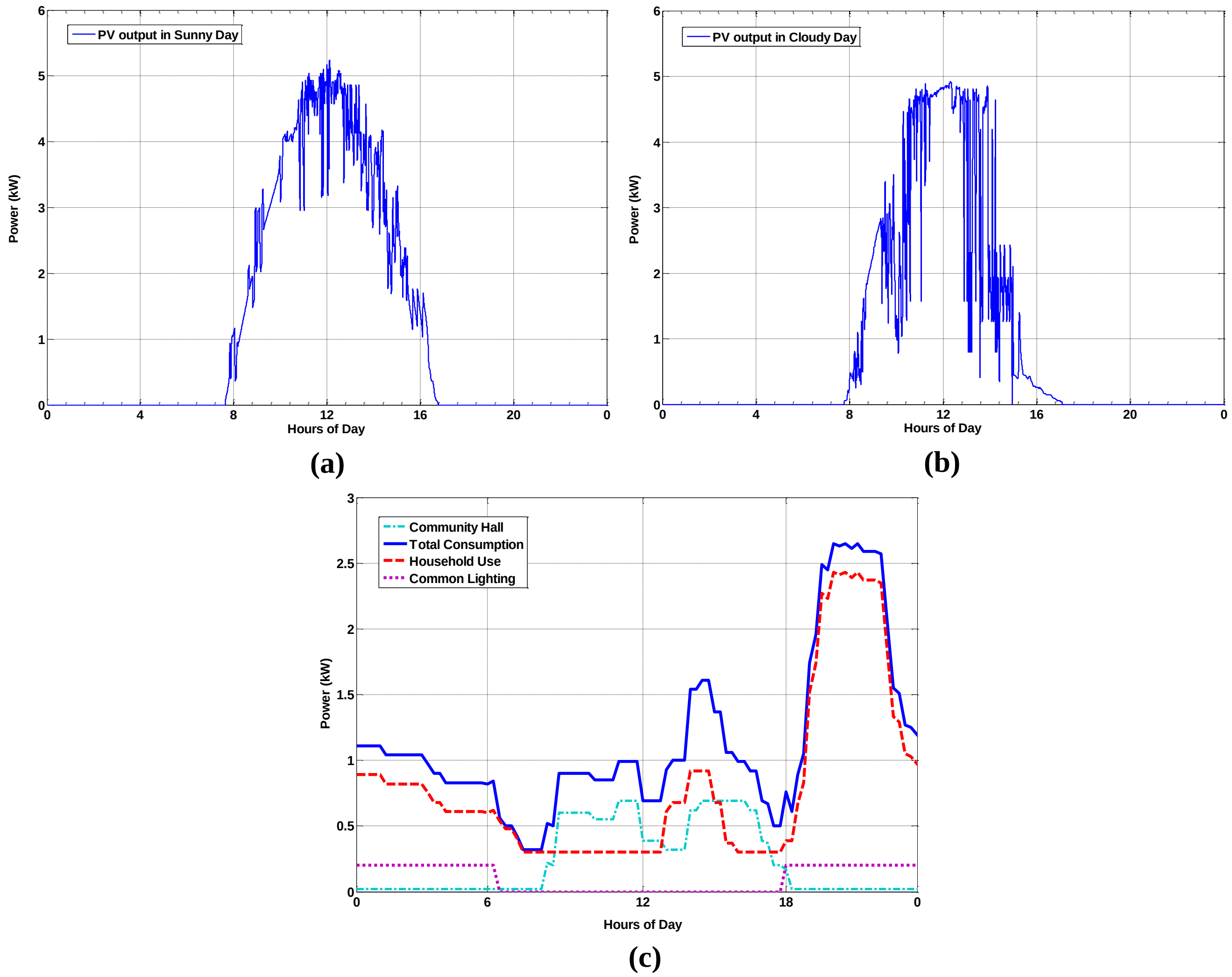

Fig. 16 The simulated PV output for (a) sunny, (b) cloudy and (c) Estimated load profiles of the target rural site in Sarawak

A. Simulation Results

The simulation was conducted for four different HESS topology settings: (1) battery only, (2) Passive HESS, (3) SC semi-active HESS and (4) Three-level HESS. An example of the Matlab Simulink model used in this work is shown in Fig. 17. The model parameters used in the simulations are tabulated in Table 1. For a fair comparison, the primary LA battery bank was kept identical for the four different cases and the capacities for the complementary ESS module are as listed in Table 1.

Table 1 Model Parameters for Different HESS under simulation

HESS System Topology	Primary Battery Capacity (Ah)	Complementary ESS Capacity
Battery-only	1000Ah (LA)	-
Passive HESS	1000Ah (LA)	1000F (SC)
SC semi-active HESS	1000Ah (LA)	1000F (SC)
Three-level HESS	1000Ah (LA)	100Ah (Li-ion) 200F (SC)

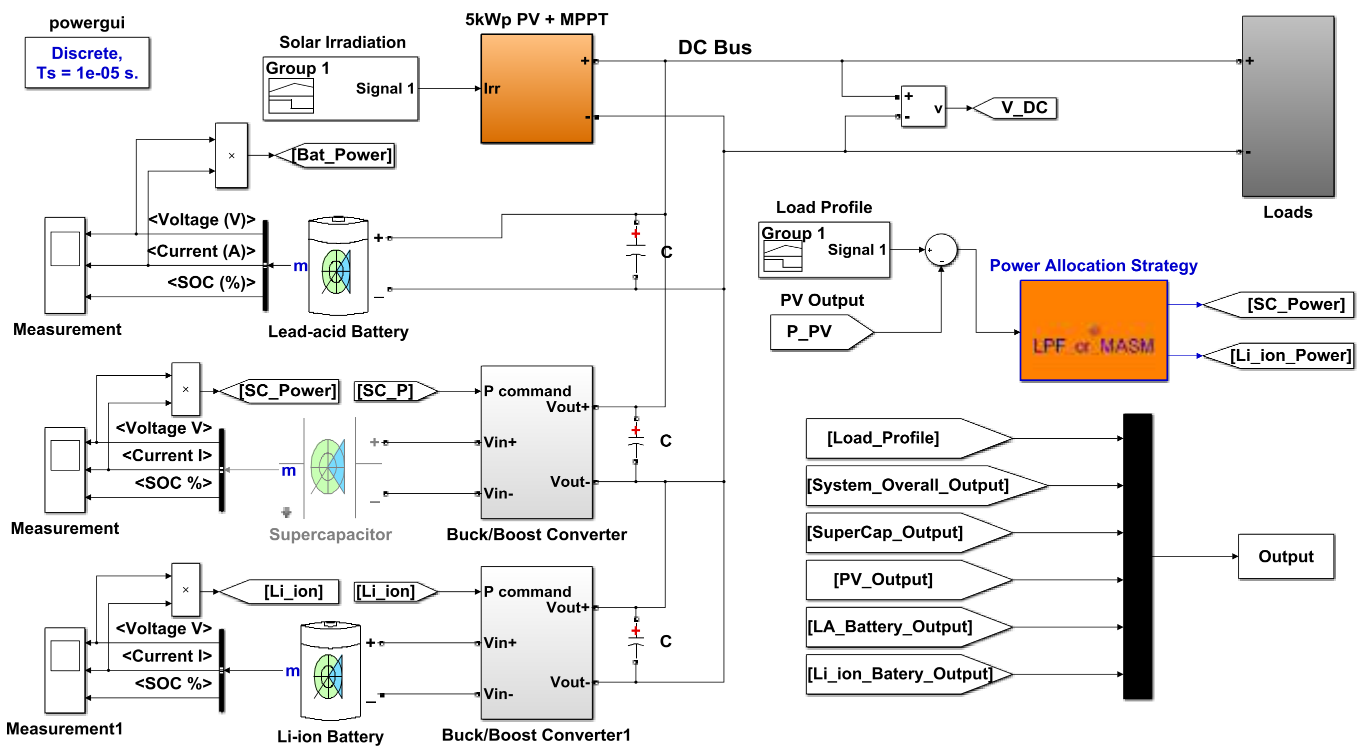

Fig. 17 The Matlab Simulink model of the standalone PV power system with three-level active HESS

The simulated current profiles of the different HESS settings for sunny day and cloudy day are illustrated in Fig. 18. The graphs on the left (Fig. 18(a), (c), (e), (g)) show the 24-hours current profiles of the net power demand (black line) and primary battery (red line) for the sunny day scenario, while the graphs on the right (Fig. 18(b), (d), (f), (h)) show the simulation results for cloudy day scenario. The battery-only setting illustrates how the battery is loaded into standalone PV power system over 24 hours. As the only ESS in the system, the battery bank is required to absorb all current fluctuations from the PV intermittence output and variation in electricity demand. This severe loading condition creates additional stresses on battery and accelerates the deterioration of the battery. In passive HESS settings, the passively connected SC absorbs part of the current fluctuations. However, the improvement in battery current profiles is insignificant compared to SC semi-active HESS and three-level HESS topologies. In SC semi-active HESS, the time constant of the low-pass filter is set to 300 seconds.

Significantly smoothed batter current profiles can be observed in Fig. 18(e) and (f). As for the three-level HESS, the combination of SC and Li-ion battery as the complementary ESS module removed the majority of the current fluctuations while at the same time, the Li-ion battery module absorbs part of the power demand which can be set by the scaling factor W_1. The power allocation strategy used in the three-level HESS is a cascaded low-pass filter as shown in Fig. 15. The time constants are set to 300 seconds and 150 seconds, with a scaling factor W_1 of 0.85, which indicates that the Li-ion battery module is designed to absorb the medium frequency fluctuation as well as supply 15% of the average power demand.

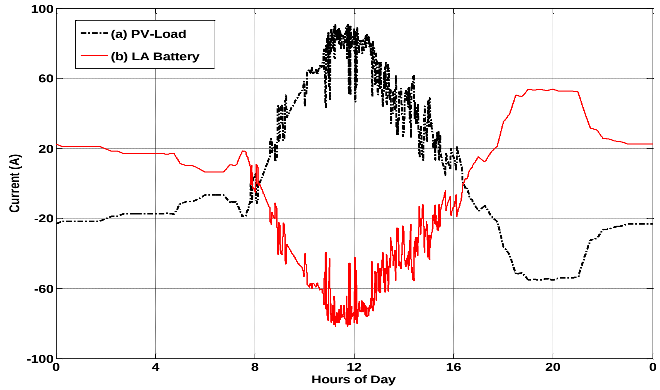

(a) Battery-only (Sunny day)

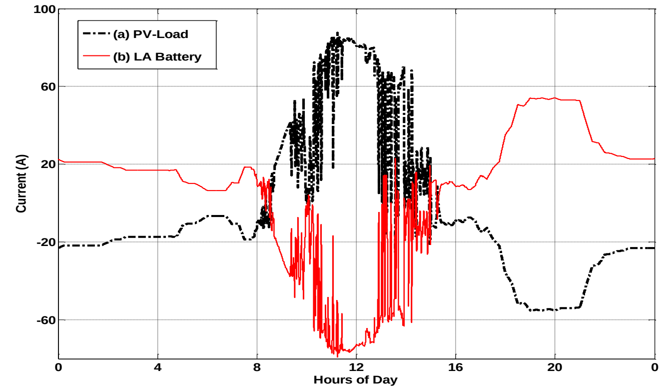

(b) Battery-only (Cloudy day)

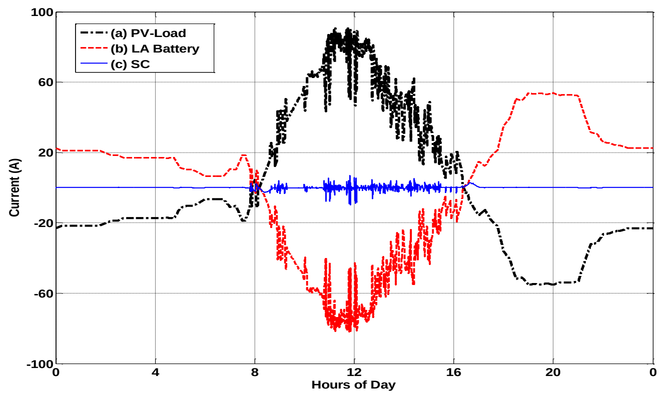

(c) Passive HESS (Sunny day)

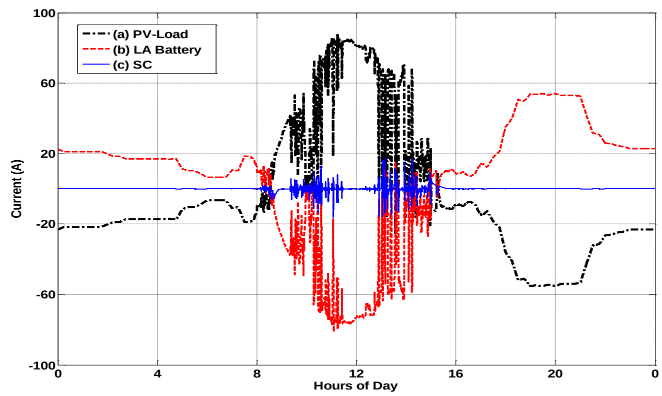

(d) Passive HESS (Cloudy day)

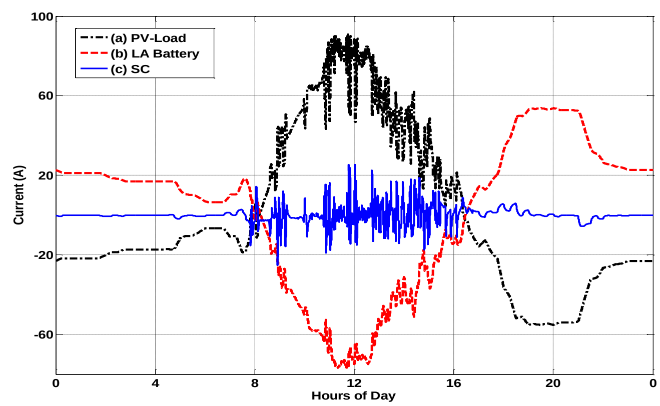

(e) SC Semi-active HESS (Sunny day)

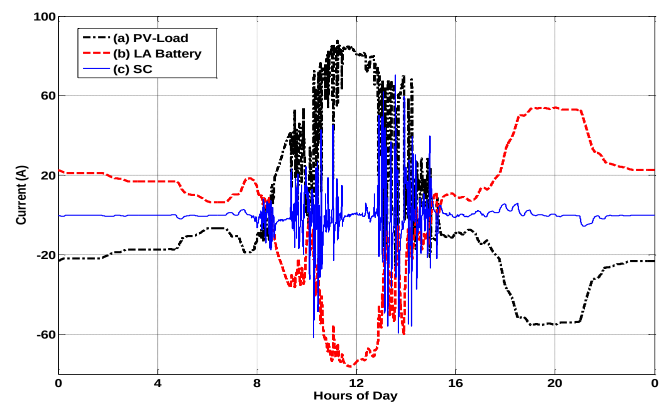

(f) SC Semi-active HESS (Cloudy day)

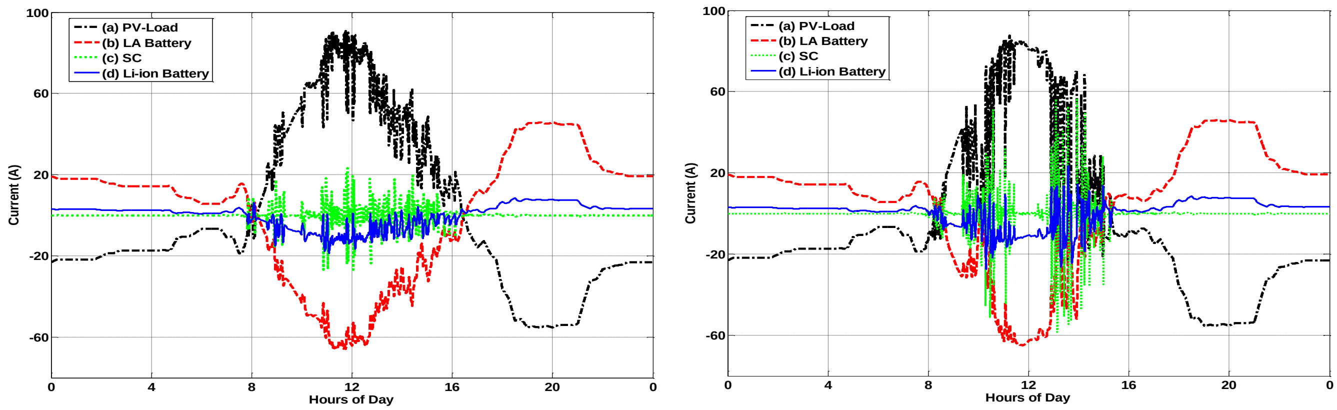

(g) Three-level HESS (Sunny day)

(h) Three-level HESS (Cloudy day)

Fig. 18 Simulated current profiles for HESS topologies under test

Fig. 19 depicts the state-of-charge (SoC) variation in SC for passive HESS, semi-active HESS, and three-level HESS respectively. With the capacity of 1000 Farad in passive HESS and semi-active HESS, only less than 10% of the SoC is utilized because of the shared terminal voltage with battery. On the other hand, the decoupled SC terminal voltage with DC/DC interface in semi-active topology, approximately 55% of the SoC is utilized for both sunny and cloudy conditions. As for the three-level HESS, the SoC variation ranges from 25% for sunny day and 55% for cloudy day, with a capacity of 200 Farad. Since the lifetime of SC normally is much longer than Li-ion battery and its installation price is also higher, there is a tradeoff between SC semi-active HESS and three-level HESS. In long-term applications, the three-level HESS needs to replace Li-ion battery regularly while semi-active HESS would not need it. Conversely, in short-term applications, the lifetime of Li-ion battery would satisfy the requirements and effectively prolongs the primary battery lifetime as same as semi-active HESS which requires 5 times more SC installation with a much higher price. Thus it can be concluded that the SC semi-active HESS is suitable for the long-term applications and the three-level HESS is suitable for the short-term applications.

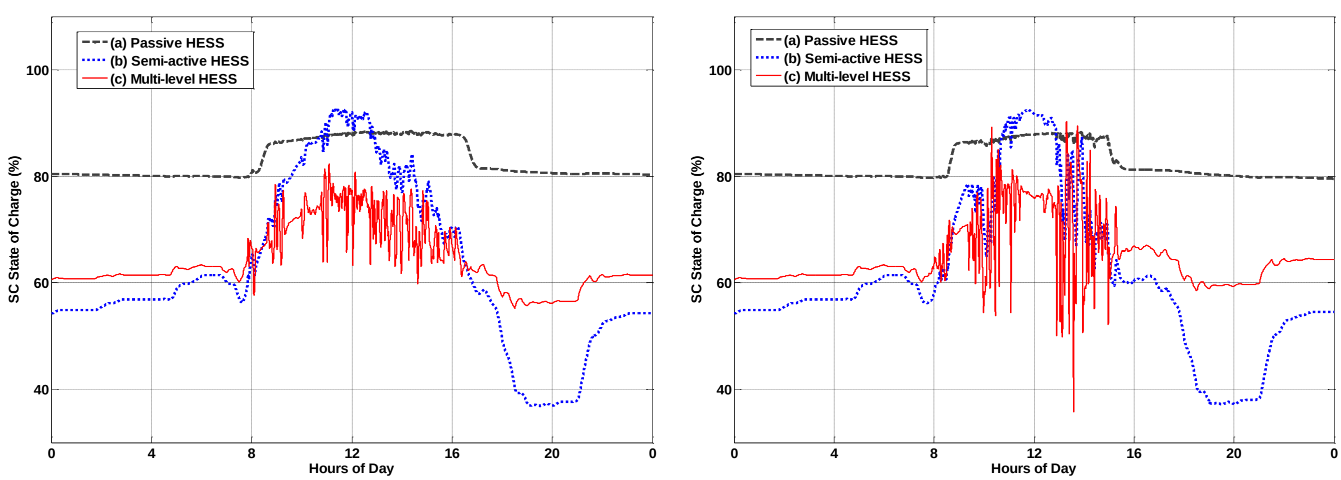

(a) Sunny day

(b) Cloudy day

Fig. 19 SoC variations of SC throughout the day in three different HESSs

B. Battery Health Cost Analysis

The simulation results presented above demonstrate the effectiveness of different HESS in mitigating the primary battery stress compared to the conventional battery-only system. To quantify the performance of the selected HESS topologies, a battery health cost function is developed as shown in equation (32) [50]:

$$Cost(T) = \sum_{t=0}^{T} n_1[i_b(t)]^2 + n_2\left|\frac{di_b(t)}{dt}\right| + n_3\big[max\big(b(t)\big) - min\big(b(t)\big)\big]^2 + n_4\begin{vmatrix}1 \ ;if\ [i_b(t)\cdot i_b(t-1) < 0] \\ 0 \ ;if\ [i_b(t)\cdot i_b(t-1) \geq 0]\end{vmatrix} + n_5 T_{year} \quad (32)$$

where T is the total operating time, $i_b(t)$ is the battery current, $b(t)$ is the battery SoC, while the n_1, n_2, n_3, n_4 and n_5 are positive constants. Five life-limiting factors are considered based on the cycle life characteristics of LA battery. The first term quantifies the impact of charge/discharge rate. The second term penalizes battery health due to current fluctuation. The third term considers the impact of deep discharge [51]. The fourth term quantifies the impact of charge/discharge transition and the fifth term indicates the calendar life of LA battery. The coefficient n_2 and n_4 are set to 0.3 indicating the strong negative impact of current fluctuation and frequent charge-discharge transitions due to the intermittent solar power. While n_1 and n_3 are set to 0.15 and 0.2 respectively to quantify the damaging impacts of charge/discharge rate and deep-discharge. The effect of calendar life n_5 is usually much lower compared to the other factors and therefore it is set to 0.05. Although the LA battery aging process is a rather complex chemical phenomenon that is difficult to be accurately quantified, the formulated cost function intends to relatively measure the impact on battery health for comparison among the HESS under consideration.

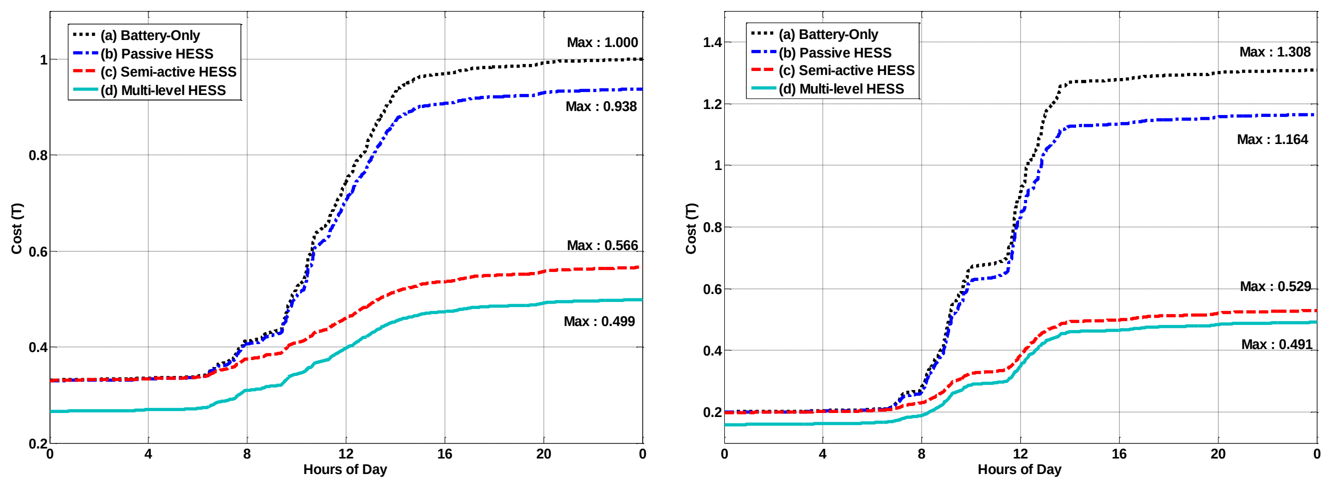

(a) Daily battery health cost (Sunny day) **(b) Daily battery health cost (Cloudy day)**

Fig. 20 Normalised cumulative cost function throughout the day for (a) sunny day and (b) cloudy day

Fig. 20 shows the normalized cumulative battery health costs of the different HESS settings. The results indicate that the three-level HESS reduces about 50% of the battery health cost compared to conventional battery-only PV power system in sunny day condition. Followed by the SC semi-active HESS, it demonstrates 43.4% reduction in sunny day, while only 6.2% reduction in battery health cost for passive HESS. Setting the battery health cost battery-only setting in sunny day as the reference, the battery-only system in cloudy day condition is 1.308 which is 30.8% more than the same setting in sunny day. This is because the relatively heavier PV power fluctuation in cloudy day has a larger impact on battery health, thus higher battery health cost. By comparing the battery health cost in a cloudy day condition, the three-level HESS manages to reduce the battery health cost by nearly 62.5%, followed by a reduction of 59.6% in SC semi-active HESS, and 11% reduction in passive HESS setting.

Finally, the estimated annual battery cost (365 days) for different systems and corresponding cost reduction are calculated and presented in Table 2. Since the SC lifetime is nearly infinite, it is not considered in the annual operating cost of the ESS in standalone PV power system. The passive HESS reduces the battery cost by 6.3% and 10.8% respectively for sunny and cloudy days, while both SC semi-active HESS and three-level HESS demonstrate significant ESS cost reduction of about 43% on a sunny day and 60% on a cloudy day. Despite the higher upfront battery cost (LA and Li-ion) in three-level HESS, it only requires 20% of the SC capacity compared to other HESSs.

Table 2 Financial analysis under different modes

Operation mode	Weather condition	Battery Capacity (kWh)	Initial Cost[1] ($)	Battery Health Cost Cost(T)[2]	Estimated Life Cycle	Cost / cycle ($)	Estimated Annual Battery Cost ($)	Cost Reduction[4]
LA Battery-only	Sunny	48 (LA)	12288	1.000	500	24.58	8971.70	0
	Cloudy	48 (LA)	12288	1.308	382	32.17	11742.05	0
Passive HESS (SC 1000F)	Sunny	48 (LA)	12288	0.938	533	23.50	8577.5	4.4%
	Cloudy	48 (LA)	12288	1.164	429	28.64	10453.6	11%
SC semi-active HESS (SC 1000F)	Sunny	48 (LA)	12288	0.566	883	13.92	5080.8	43.4%
	Cloudy	48 (LA)	12288	0.529	945	13.00	4745.00	59.6%
Multi-level HESS (SC 200F)	Sunny	48 (LA)	12288	0.499	1002	13.26	4839.9 + 255.5(Li-ion) = 5095.4	43.2%
		4.8 (Li-ion)	1392	-	2000[3]	0.70		
	Cloudy	48 (LA)	12288	0.491	1018	12.07	4405.55 + 255.5(Li-ion) = 4661.05	60.3%
		4.8 (Li-ion)	1392	-	2000[3]	0.70		

#Note 1 – Initial cost of LA battery ($256/kWh) and Li-ion battery ($290/kWh) are considered. [45]
#Note 2 – Typical life cycle / Cost of battery utilization; (typical life cycle for LA – 500 cycles, Li-ion – 4000 cycles and SC >100,000 cycles) [45]
#Note 3 – Estimated to perform 50% of the expected lifecycles of the Li-ion battery when LA battery is replaced
#Note 4 – Percentage cost reduction is calculated based on battery-only system.

V. EXPERIMENT VERIFICATION

A. Testbed Setup

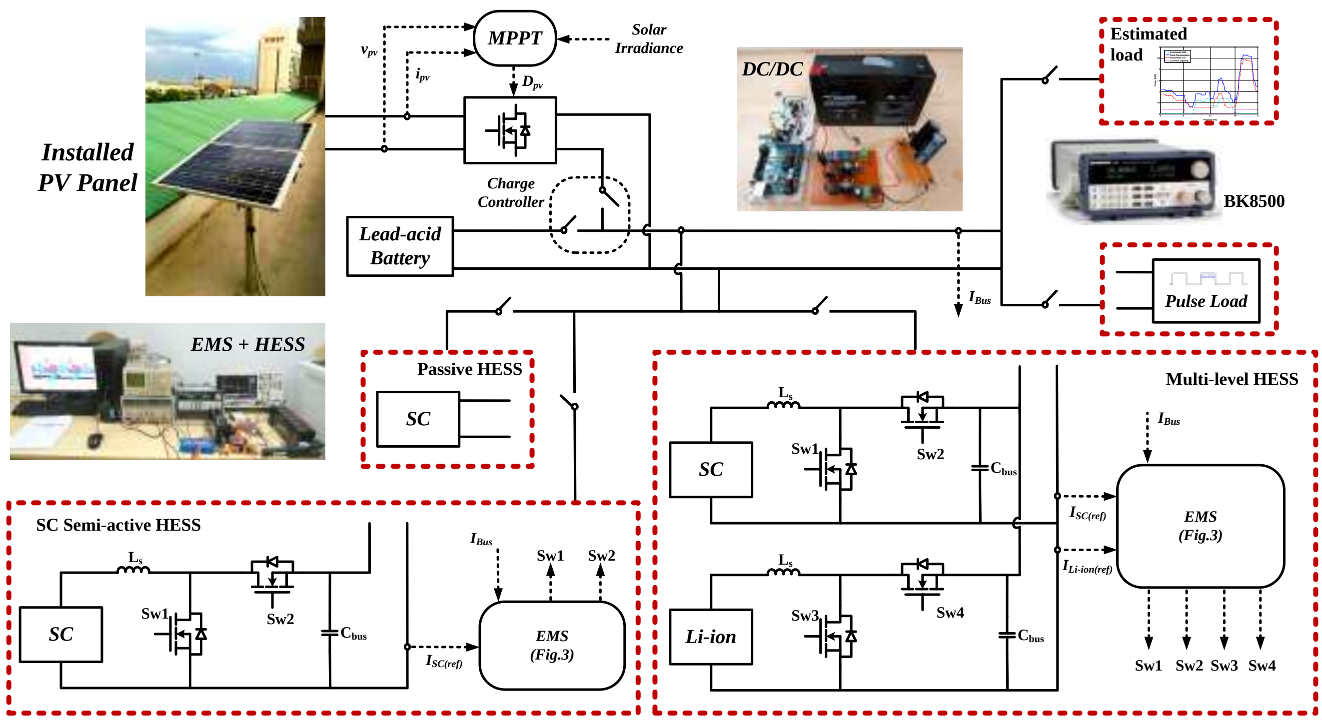

Fig. 21 Experiment setup of selected HESS topologies

To demonstrate the feasibility of the selected HESS topologies and to verify the simulation analysis presented in the previous section, scale-down prototypes of the selected HESSs were designed as illustrated in Fig. 21 and a series of experiments were implemented. The prototype was tested for pulsed load cycling and integrated to a 15W standalone PV power system for actual testing. A programmable DC electronic load (BK Precision BK8500) was used to emulate the pulsed load as well as the estimated load profiles. A 15 watts solar panel was used to generate the PV input power. The current flows in battery and SC module were measured with current sensors (ACS712) and logged by using the NI USB-6008 data acquisition device. The power allocation and control algorithm was controlled by Arduino (ATMEGA328P). Table 2 presents a summary of the experiment parameters.

Table 1 Experimental testbed parameters

System Parameters	Passive HESS	SC semi-active HESS	Three-level HESS
PV panel peak power		15W	
Daily load energy consumption		0.4 kWh	
LA Battery nominal voltage		6V	
LA Battery capacity		30Ah	
SC Capacitance	-	50F	25F
SC Equivalent Series Resistance	-	0.001Ω	0.001Ω
Li-ion Battery nominal voltage	-	-	12V
Li-ion Battery capacity	-	-	6Ah

B. Pulse Load Responses

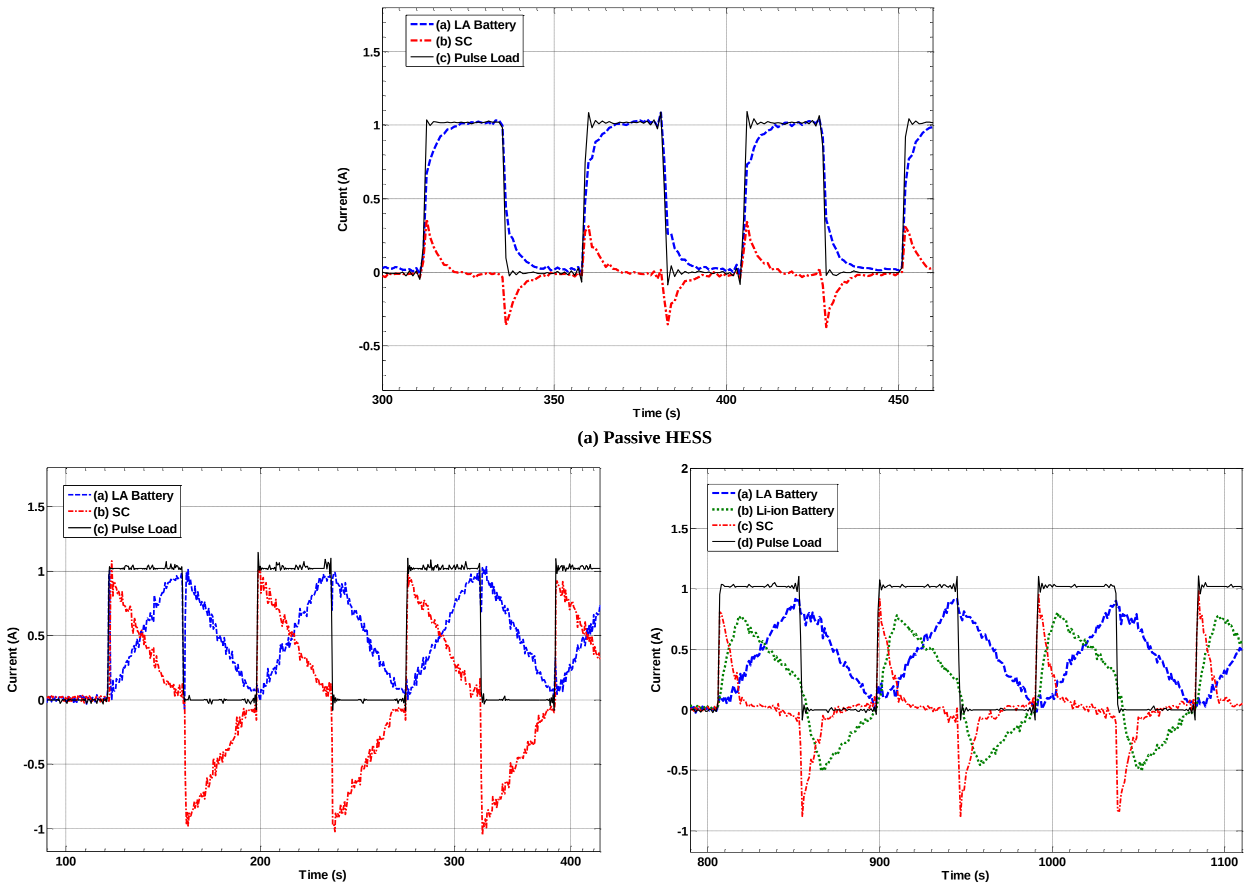

(a) Passive HESS

(b) SC semi-active HESS

(c) Three-level HESS

Fig. 22 Responses to pulsed load of HESSs under experiment test

A repetitive pulsed current profile with amplitude of 1 Ampere, period of 120 seconds, and 50 percent in duty ratio was generated by using BK8500. Fig. 22 shows the responses of battery and SC currents in each selected HESS under test. In passive HESS (Fig. 22(a)), the SC responded instantaneously to the step change in current, while the battery picked up slowly with a time constant of about 1.5 seconds. In SC semi-active HESS, an Arduino controlled bi-directional buck/boost DC/DC converter was used to control the current flow in SC module with a simple digital LPF to allocation current among SC and battery modules. As seen from Fig. 22(b), the SC responded quickly to the step change in current and allowed the battery to gently supply/absorb the current change. The current responses of the three-level HESS, Fig. 22(c), also enabled the primary battery to gently supply/absorb the changes but with notably a lower peak current due to the fact that the Li-ion battery module shares part of the current demand that can be determined by setting the scaling factor (set at 0.85 for this experiment). The experimental results of pulsed load testing match the simulations results presented in this paper.

C. Standalone PV Power System Test

The HESS daily operational testing with 15W standalone PV power system was carried out on HESSs under test separately on four different partly cloudy days at Swinburne University of Technology Sarawak Campus, Kuching, Malaysia. The net current demand ($I_{PV} - I_{Load}$, black line), primary battery current (red line) and SC current (blue line) are depicted in Fig. 23.

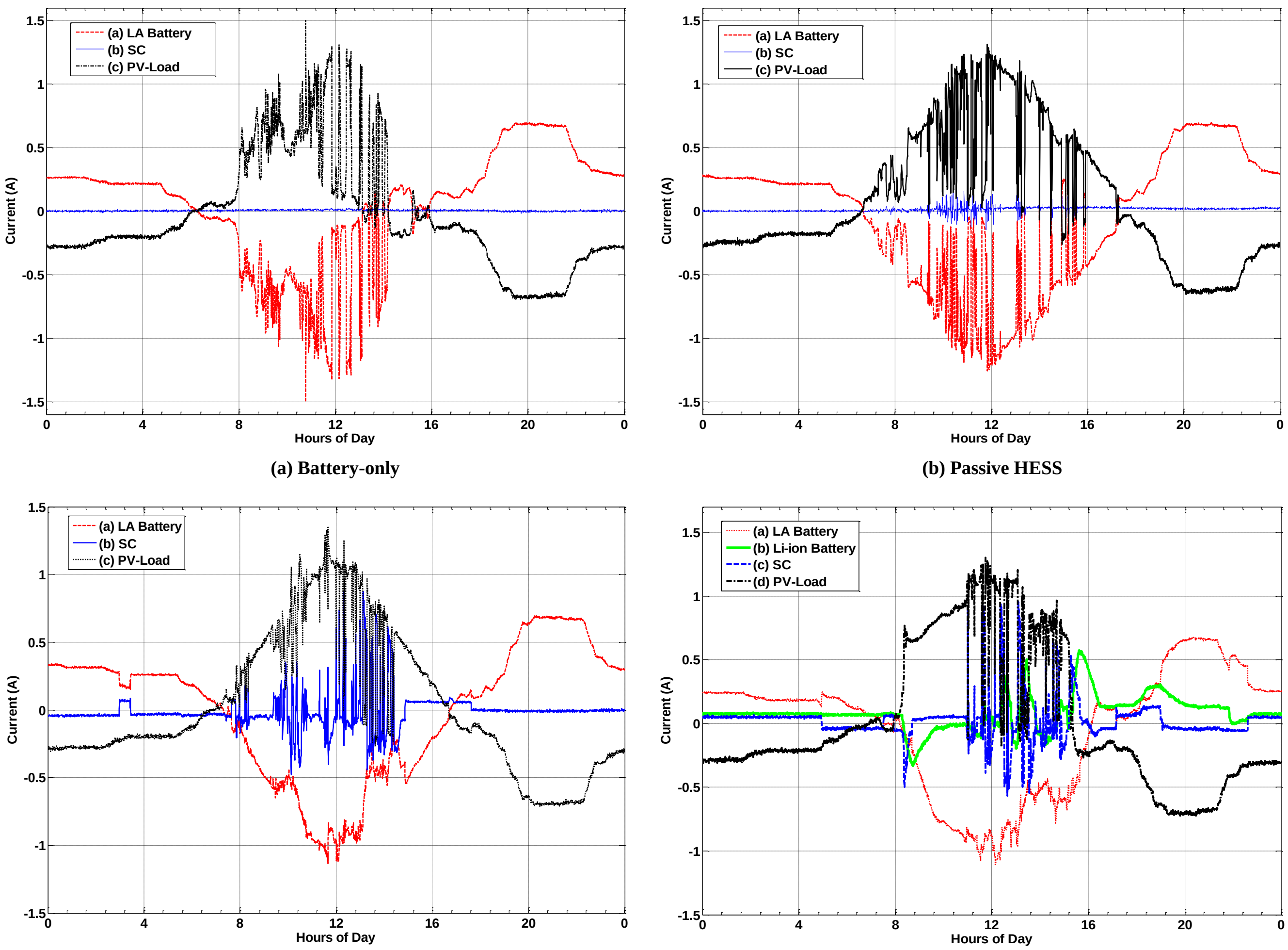

(a) Battery-only

(b) Passive HESS

(c) SC semi-active HESS

(d) Three-level HESS

Fig. 23 Experimental results on battery and SC current profiles in standalone PV power system

Minimal mitigation of current fluctuation is demonstrated in passive HESS (Fig. 23(b)), while SC semi-active HESS and three-level HESS remove the majority of the primary battery current fluctuation as seen from Fig. 23(c) for SC semi-active HESS and Fig. 23(d) for three-level HESS. In addition, the three-level HESS shares part of the current demand with Li-ion battery module with a pre-determined scaling factor. The experimental results demonstrate the feasibility of the HESS under test in standalone PV power system and validate the simulation analysis presented in this paper.

VI. CONCLUSION

Standalone PV power system with battery energy storage has been one of the preferred choices in off-grid rural electrification widely available solar energy and the technology advances in sustainable technologies. However, the nature of solar energy causes the additional impact on the battery which accelerates the deterioration of battery performance and cycle life. Hybridization of different energy storage devices has been proposed by researchers aiming to extend the service life of the battery in many high energy applications over the past decades. This paper presented a comprehensive review of hybrid energy storage system and their feasibility on standalone PV power system, specifically for off-grid rural electrification. Three potential hybrid energy storage system topologies, the associated power allocation strategy, and control system have been discussed in this paper, followed by numerical simulation and experimental verification. Matlab Simulink models of the selected hybrid energy storage systems are developed and simulated with actual solar irradiance data and estimated load profile to evaluate the effectiveness in mitigating battery stress. The simulation analysis and results have been verified by experiments with the developed prototype of hybrid energy storage system under consideration. Simulation results, battery health cost and financial analyses, and empirical outcomes suggest that the combination of active secondary energy storage with the passive primary battery could be the optimal setting for standalone PV power system applications.

REFERENCES

[1] International Energy Agency, "World Energy Outlook 2017," *IEA*, vol. Chapter 1, 2017.

[2] J. Sachs and O. Sawodny, "A Two-Stage Model Predictive Control Strategy for Economic Diesel-PV-Battery Island Microgrid Operation in Rural Areas," *IEEE Trans. Sustain. Energy*, vol. 7, no. 3, pp. 1–11, 2016.

[3] REN21, "Renewables 2017: global status report (GSR)," *Renew. Energy Policy Netw. 21st century*, pp. 1–302, 2017.

[4] (IEA) International Energy Agency, *Trends 2016 in Photovoltaic Applications. Survey Report of Selected IEA Countries between 1992 and 2015*. 2016.

[5] L. R. Valer, A. R. A. Manito, T. B. S. Ribeiro, R. Zilles, and J. T. Pinho, "Issues in PV systems applied to rural electrification in Brazil," *Renew. Sustain. Energy Rev.*, vol. 78, no. April, pp. 1033–1043, 2017.

[6] J. Linssen, P. Stenzel, and J. Fleer, "Techno-economic analysis of photovoltaic battery systems and the influence of different consumer load profiles," *Appl. Energy*, vol. 185, pp. 2019–2025, 2017.

[7] J. Hoppmann, J. Volland, T. S. Schmidt, and V. H. Hoffmann, "The economic viability of battery storage for residential solar photovoltaic systems - A review and a simulation model," *Renew. Sustain. Energy Rev.*, vol. 39, pp. 1101–1118, 2014.

[8] R. Dufo-lópez, J. M. Lujano-rojas, and J. L. Bernal-agustín, "Comparison of different lead – acid battery lifetime prediction models for use in simulation of stand-alone photovoltaic systems," *Appl. Energy*, vol. 115, pp. 242–253, 2014.

[9] W. Jing, C. H. Lai, W. S. H. Wong, and M. L. D. Wong, "Smart hybrid energy storage for stand-alone PV microgrid: Optimization of battery lifespan through dynamic power allocation," in *Power and Energy Engineering Conference (APPEEC), IEEE PES Asia-Pacific*, 2015, vol. 2016–Janua, pp. 3–7.

[10] N. R. Tummuru, M. K. Mishra, and S. Srinivas, "Dynamic Energy Management of Hybrid Energy Storage System With High-Gain PV Converter," vol. 30, no. 1, pp. 150–160, 2014.

[11] F. Li, K. Xie, and J. Yang, "Optimization and Analysis of a Hybrid Energy Storage System in a Small-Scale Standalone Microgrid for Remote Area Power Supply (RAPS)," *Energies*, vol. 8, pp. 4802–4826, 2015.

[12] A. González, E. Goikolea, J. A. Barrena, and R. Mysyk, "Review on supercapacitors: Technologies and materials," *Renew. Sustain. Energy Rev.*, vol. 58, pp. 1189–1206, 2016.

[13] S. K. ; Mishra and M. Kumar, "A Supervisory Power Management System for a Hybrid MicrogridWith HESS," *IEEE Trans. Ind. Electron.*, vol. 64, no. 5, pp. 3640–3649, 2017.

[14] H. Samani and X. Fernando, "Battery Current's Fluctuations Removal in Hybrid Energy Storage System Based on Optimized Control of Supercapacitor Voltage," *IEEE Embed. Syst. Lett.*, vol. 8, no. 3, pp. 53–56, 2016.

[15] D. B. Wickramasinghe Abeywardana, B. Hredzak, and V. G. Agelidis, "A Fixed-Frequency Sliding Mode Controller for a Boost-Inverter-Based Battery-Supercapacitor Hybrid Energy Storage System," *IEEE Trans. Power Electron.*, vol. 32, no. 1, pp. 668–680, 2017.

[16] X. Wang, D. Yu, S. Le, Z. Zhao, and P. Wilson, "A novel controller of a battery-supercapacitor hybrid energy storage system for domestic applications," *Energy Build.*, vol. 141, pp. 167–174, 2017.

[17] Q. Xu, S. Member, X. Hu, P. Wang, S. Member, J. Xiao, P. Tu, S. Member, and C. Wen, "A Decentralized Dynamic Power Sharing Strategy for Hybrid Energy Storage System in Autonomous DC Microgrid," *IEEE Trans. Ind. Electron.*, vol. 64, no. 7, pp. 5930–5941, 2017.

[18] Y. Kim and V. Raghunathan, "Design and Management of Battery-Supercapacitor Hybrid Electrical Energy Storage Systems for Regulation Services," *IEEE Trans. Multi-Scale Comput. Syst.*, vol. 3, no. 1, pp. 12–24, 2017.

[19] Z. Cabrane, M. Ouassaid, and M. Maaroufi, "Analysis and evaluation of battery-supercapacitor hybrid energy storage system for photovoltaic installation," *Int. J. Hydrogen Energy*, vol. 41, no. 45, pp. 20897–20907, 2016.

[20] J. P. Zheng, T. R. Jow, and M. S. Ding, "Hybrid power sources for pulsed current applications," *IEEE Trans. Aerosp. Electron. Syst.*, vol. 37, no. 1, pp. 288–292, 2001.

[21] R. A. Dougal, S. Member, S. Liu, and R. E. White, "Power and Life Extension of Battery – Ultracapacitor Hybrids," *IEEE Trans. Components Packag. Technol.*, vol. 25, no. 1, pp. 120–131, 2002.

[22] D. Shin, Y. Kim, Y. Wang, N. Chang, and M. Pedram, "Constant-current regulator-based battery-supercapacitor hybrid architecture for high-rate pulsed load applications," *J. Power Sources*, vol. 205, pp. 516–524, 2012.

[23] B. Hredzak, V. G. Agelidis, and G. D. Demetriades, "A low complexity control system for a hybrid DC power source based on ultracapacitor-lead-acid battery configuration," *IEEE Trans. Power Electron.*, vol. 29, no. 6, pp. 2882–2891, 2014.

[24] Z. Song, J. Hou, H. Hofmann, J. Li, and M. Ouyang, "Sliding-mode and Lyapunov function-based control for battery / supercapacitor hybrid energy storage system used in electric vehicles," *Energy*, vol. 122, pp. 601–612, 2017.

[25] Z. Cabrane, M. Ouassaid, and M. Maaroufi, "Battery and supercapacitor for photovoltaic energy storage : a fuzzy logic management," *IET Renew. Power Gener.*, vol. 11, no. 4, pp. 1157–1165, 2017.

[26] A. Aktas, K. Erhan, S. Ozdemir, and E. Ozdemir, "Experimental investigation of a new smart energy management algorithm for a hybrid energy storage system in smart grid applications," *Electr. Power Syst. Res.*, vol. 144, pp. 185–196, 2017.

[27] P. Golchoubian and N. L. Azad, "Real-Time Nonlinear Model Predictive Control of a Battery-Supercapacitor Hybrid Energy Storage System in Electric Vehicles," *IEEE Trans. Veh. Technol.*, vol. 9545, no. c, pp. 1–12, 2017.

[28] A. Kuperman, I. Aharon, S. Malki, and A. Kara, "Design of a semiactive battery-ultracapacitor hybrid energy source," *IEEE Trans. Power Electron.*, vol. 28, no. 2, pp. 806–815, 2013.

[29] C. Ye, S. Miao, Q. Lei, and Y. Li, "Dynamic Energy Management of Hybrid Energy Storage Systems with a Hierarchical Structure," *Energies*, 2016.

[30] F. Ciccarelli, G. Clemente, and D. Iannuzzi, "Energy storage management control based on supercapacitors using a modular multilevel inverter topology for electrical vehicles," *4th Int. Conf. Clean Electr. Power Renew. Energy Resour. Impact, ICCEP 2013*, pp. 170–176, 2013.

[31] Y. Kim, J. Koh, Q. Xie, Y. Wang, N. Chang, and M. Pedram, "A scalable and flexible hybrid energy storage system design and implementation," *J. Power Sources*, vol. 255, pp. 410–422, 2014.

[32] Y. Ye and K. W. E. Cheng, "Analysis and Design of Zero-Current Switching Switched-Capacitor Cell Balancing

Circuit for Series-Connected Battery/Supercapacitor," *IEEE Trans. Veh. Technol.*, vol. 67, no. 2, pp. 948–955, 2018.

[33] W. Jing, C. H. Lai, W. S. H. Wong, and M. L. D. Wong, "Battery-supercapacitor hybrid energy storage system in standalone DC microgrids: areview," *IET Renew. Power Gener.*, vol. Vol. 11, no. Iss. 4, pp. 461–469, 2017.

[34] L. W. Chong, Y. W. Wong, R. K. Rajkumar, and D. Isa, "An optimal control strategy for standalone PV system with Battery-Supercapacitor Hybrid Energy Storage System," *J. Power Sources*, vol. 331, pp. 553–565, 2016.

[35] H. Zhou, T. Bhattacharya, D. Tran, T. S. T. Siew, and A. M. Khambadkone, "Composite Energy Storage System Involving Battery and UltracapacitorWith Dynamic Energy Management in Microgrid Applications," *IEEE Trans. POWER Electron.*, vol. 26, no. 3, pp. 923–930, 2011.

[36] X. Feng, G. S. Member, H. B. Gooi, S. Member, and S. X. Chen, "Hybrid Energy Storage With Multimode Fuzzy Power Allocator for PV Systems," *IEEE Trans. Sustain. Energy*, vol. 5, no. 2, pp. 389–397, 2014.

[37] H. Yin, C. Zhaor, M. Li, C. Ma, and M.-Y. Chow, "A Game Theory Approach to Energy Management of An Engine–Generator/Battery/Ultracapacitor Hybrid Energy System," *IEEE Trans. Ind. Electron.*, vol. 63, no. 7, pp. 4266–4277, 2016.

[38] Y. Y. Chia, L. H. Lee, N. Shafiabady, and D. Isa, "A load predictive energy management system for supercapacitor-battery hybrid energy storage system in solar application using the Support Vector Machine," *Appl. Energy*, vol. 137, pp. 588–602, 2015.

[39] R. T. Bambang, A. S. R, and C. J. Dronkers, "Energy Management of Fuel Cell/Battery/Supercapacitor Hybrid Power Sources Using Model Predictive Control," *IEEE Trans. Ind. Informatics*, vol. 3203, no. 4, pp. 1–1, 2014.

[40] M. Choi, S. Kim, and S. Seo, "Energy Management Optimization in a Battery / Supercapacitor Hybrid Energy Storage System," *IEEE Trans. Smart Grid*, vol. 3, no. 1, pp. 463–472, 2012.

[41] H. Saboori, R. Hemmati, S. Mohammad, S. Ghiasi, and S. Dehghan, "Energy storage planning in electric power distribution networks – A state- of-the-art review," *Renew. Sustain. Energy Rev.*, vol. 79, no. December 2016, pp. 1108–1121, 2017.

[42] R. Atia and N. Yamada, "Distributed renewable generation and storage system sizing based on smart dispatch of microgrids," *Energies*, vol. 9, no. 3, 2016.

[43] D. E. Olivares, C. A. Canizares, and M. Kazerani, "A centralized energy management system for isolated microgrids," *IEEE Trans. Smart Grid*, vol. 5, no. 4, pp. 1864–1875, 2014.

[44] Z. Song, H. Hofmann, J. Li, X. Han, X. Zhang, and M. Ouyang, "A comparison study of different semi-active hybrid energy storage system topologies for electric vehicles," *J. Power Sources*, vol. 274, pp. 400–411, 2015.

[45] V. I. Herrera, H. Gazta, A. Milo, and A. Saez-de-ibarra, "Optimal Energy Management and Sizing of a Battery – Supercapacitor-Based Light Rail Vehicle With a Multiobjective Approach," *IEEE Trans. Ind. Appl.*, vol. 52, no. 4, pp. 3367–3377, 2016.

[46] S. Goel and R. Sharma, "Performance evaluation of stand alone , grid connected and hybrid renewable energy systems for rural application : A comparative review," *Renew. Sustain. Energy Rev.*, vol. 78, no. May, pp. 1378–1389, 2017.

[47] W. Jing, C. H. Lai, W. S. H. Wong, and M. L. D. Wong, "Dynamic power allocation of battery-supercapacitor hybrid energy storage for standalone PV microgrid applications," *Sustain. Energy Technol. Assessments*, vol. 22, pp. 55–64, 2017.

[48] T. Ma, H. Yang, and L. Lu, "Development of hybrid battery-supercapacitor energy storage for remote area renewable energy systems," *Appl. Energy*, vol. 153, pp. 56–62, 2015.

[49] A. Kuperman and I. Aharon, "Battery-ultracapacitor hybrids for pulsed current loads: A review," *Renew. Sustain. Energy Rev.*, vol. 15, no. 2, pp. 981–992, 2011.

[50] W. Jing, C. H. Lai, W. S. H. Wong, and M. L. D. Wong, "Cost Analysis of Battery-Supercapacitor Hybrid Energy Storage System for Standalone PV Systems," in *4th IET Clean Energy and Technology Conference (CEAT)*, 2016, p. 9.

[51] J. Schiffer, D. Uwe, H. Bindner, T. Cronin, P. Lundsager, and R. Kaiser, "Model prediction for ranking lead-acid batteries according to expected lifetime in renewable energy systems and autonomous power-supply systems," vol. 168, pp. 66–78, 2007.